Hypoid facemilled Validation Manual

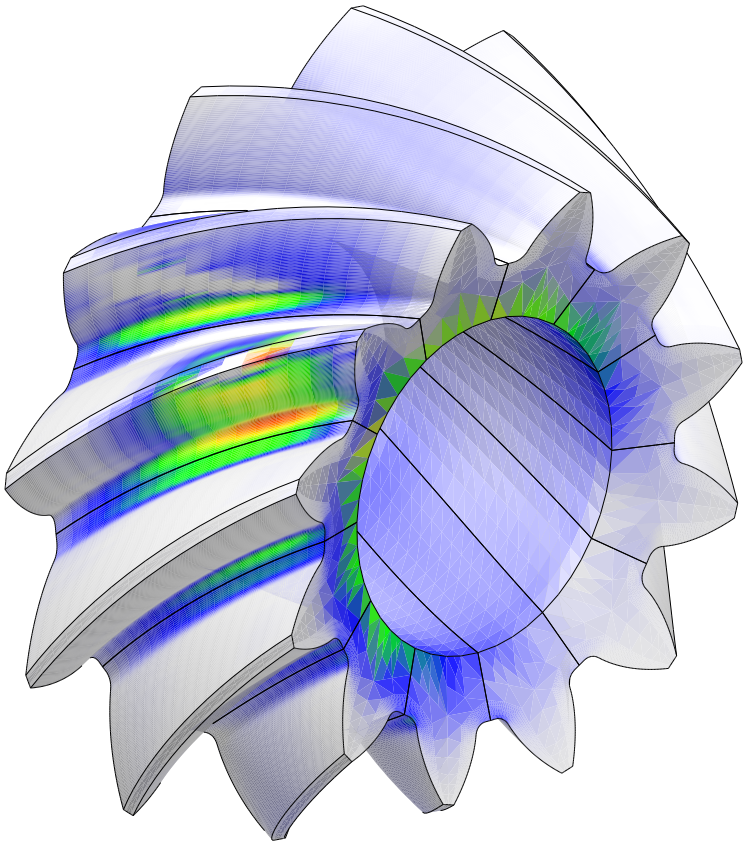

Advanced Numerical Solutions
Hilliard OH

February 25, 2003

Contents

List of Figures

List of Tables

Preface

The Hypoid facemilled computer program has been under development for many years, and is finally available for use by the gearing community. We have received active support and encouragement from many people. We would especially like to thank Timothy Krantz of the Army Research Laboratory at the NASA Glenn Research Center for his support and encouragement.

Sandeep Vijayakar, Hilliard OH
Samir Abad, Hilliard OH
February 2003

Chapter 1

Introduction

The *HypoidFaceMilled* program is used for the analysis of hypoid gear pairs. The `Users manual` describes the various features of the *HypoidFaceMilled* package. It provides detailed information to help you run the program. The `Validation manual` describes through examples some of the applications of the *HypoidFaceMilled* program.

Test cases are documented so as to study the effect of various parameters such as tip radius, tooth thickness, number of face elements and displacement order on the stresses for hypoid gears and also the convergence of the stress values for different types of mesh templates. Finally the manual discusses the application of the *HypoidFaceMilled* program related to fatigue theory and life prediction in hypoid gears.

User should read the `Users manual` before trying out the examples in the `Validation manual`. All the files referred to in the `Validation manual` are in the Working directory created during the time of installation.

Chapter 2

Convergence study

The test cases described in this chapter are meant to study the effect of various parameters such as tip radius, thickness, nfaceelems and displorder on the maximum principal normal stress for a hypoid pinion and also the convergence of the stress values for different types of mesh templates.

2.1 Running the study cases

The data for the example problem is in English units. The outputs are also in English units. Table 2.1 shows the English units for the physical quantities used to run the test cases.

Tables 2.2 through 2.10 show the data to be entered in the EDIT menu for running the test cases. No assembly errors are considered for the pinion and the gear. Also, pinion tooth modifications are not applied for these test cases. 11 time steps covering one mesh cycle were run.

Table 2.1: Units used for the test cases

Physical quantity	English
LENGTH	in
TIME	secs
ANGLE	deg or rad
MASS	$lbf.s^2/in$
MOMENT OF INERTIA	$lbf.s^2.in$
STIFFNESS	lbf/in
SPEED	RPM
TORQUE	lbf.in
YOUNGS MODULUS	lbf/in^2
DENSITY	$lbf.s^2/in^4$
LOAD	lbf
STRESSES	psi

Table 2.2: System configuration parameters

Item	Description
MODELTYPE	CALYX3D
HANDPINION	LEFT
OFFSET	0.00
ANGLE	90.00
LOADEDSIDE	CONVEX
DRIVER	PINION
MU	0.00
TORQUE	2613.33
RPM	100.00
DOASSEMBLYERRORS	FALSE

Table 2.3: Pinion common design and blank data

Item	Description
NTEETH	12
NFACEELEMENTS	4
COORDORDER	4
DISPLORDER	3
THICKNESS	0.262
OUTERCONEDIST	3.691
FACEWIDTH	1.00
FACEANGLE	22.3167
BACKANGLE	18.4333
FRONTANGLE	18.4333
SPIRALANGLE	35.00
PITCHANGLE	18.4333
PITCHAPEX	0.00
FACEAPEX	0.00
ROOTAPEX	0.00
BASESURFACETYPE	CYLINDER
BASECYLINDERDIAME	1.138
ISRACERIGID	FALSE
AXIALORDER	1
CIRCORDER	4
YOUNGSMOD	3.00E7
POISSON	0.3
DENSITY	0.3
ALPHA	0.001
BETA	1E-7
TPLFILE	Medium
MESHFILE	pinioncalyx.msh

Table 2.4: Machine parameters for concave and convex tooth side for the pinion

Item	Concave side	Convex side
RADIALSETTING	2.9478	2.80105
TILTANGLE	0.00	0.00
SWIVELANGLE	0.00	0.00
BLANKOFFSET	0.154576	-0.174262
ROOTANGLE	16.8667	16.8667
MACHCTRBACK	-0.0402306	0.0541429
SLIDINGBASE	0.116727	-0.0157093
CRADLEANGLE	63.942	53.926
RATIOROLL	3.2427	3.10518
2C	0.00	0.00
6D	0.00	0.00
24E	0.00	0.00
120F	0.00	0.00
H1	0.00	0.00
H2	0.00	0.00
H3	0.00	0.00
V1	0.00	0.00
V2	0.00	0.00
V3	0.00	0.00

Table 2.5: Cutter settings for concave and convex tooth side of a pinion

Item	Concave	Convex
POINTRADIUS	2.96562	3.07131
BLADEANGLE	18.0457	24.3374
EDGERADIUS	0.045	0.045
TYPE	Straight	Straight

Table 2.6: Gear common design and blank data

Item	Description
NTEETH	36
NFACEELEMENTS	4
COORDORDER	4
DISPLORDER	3
THICKNESS	0.15
OUTERCONEDIST	3.691
FACEWIDTH	1.00
FACEANGLE	72.50
BACKANGLE	71.5667
FRONTANGLE	71.5667
SPIRALANGLE	35.00
PITCHANGLE	71.5667
PITCHAPEX	0.00
FACEAPEX	0.00
ROOTAPEX	0.00
BASESURFACETYPE	CONE
BASECONEANGLE	61.50
BASECONEAPEX	0.00
ISRACERIGID	TRUE
YOUNGSMOD	3.00E7
POISSON	0.3
DENSITY	0.3
ALPHA	0.001
BETA	1E-7
TPLFILE	Medium
MESHFILE	gearcalyx.msh

Table 2.7: Gear Machine data for concave and convex tooth side

Item	Concave side	Convex side
RADIALSETTING	2.85995	2.85995
TILTANGLE	0.00	0.00
SWIVELANGLE	0.00	0.00
BLANKOFFSET	0.00	0.00
ROOTANGLE	67.6833	67.6833
MACHCTRBACK	0.00	0.00
SLIDINGBASE	0.00	0.00
CRADLEANGLE	59.2342	59.2342
RATIOROLL	1.05167	1.05167
2C	0.00	0.00
6D	0.00	0.00
24E	0.00	0.00
120F	0.00	0.00
H1	0.00	0.00
H2	0.00	0.00
H3	0.00	0.00
V1	0.00	0.00
V2	0.00	0.00
V3	0.00	0.00

Table 2.8: Cutter settings for concave and convex tooth side of a gear

Item	Concave	Convex
POINTRADIUS	3.0325	2.9675
BLADEANGLE	22	22
EDGERADIUS	0.001	0.001
TYPE	Straight	Straight

Table 2.9: The rim parameters for the gear

Item	Description
DORIM	TRUE
NELEMS	4
ELEMTYPE	LINEAR
AXIALORDER	1
CIRCORDER	8
NSEGS	4
ISEG	4
RA	1.75
RB	1.75
ZA	1.50
ZB	1.761

Table 2.10: Analysis Setup data

Item	Description
SEPTOL	0.005
NPROFDIVS	5
NFACEDIVS	15
DSPROF	0.005
INITIALTIME	0.0
NRANGES	1
RANGE	1
SOLMETHOD	STATIC
NTIMESTEPS	11
DELTATIME	0.005
STARTSPEEDFACTOR	1.0
STARTTORQUEFACTOR	1.0
ENDTORQUEFACTOR	1.0
SAVEPERIODICALLY	FALSE
OUTPUTRESTART	FALSE
POSTPROCWRITE	TRUE
POSTFILENAME	postproc.dat
NSTEPSWRITE	1

Table 2.11: Searchstress settings

Item	Description
COMPONENT	MAXPPLSTRESS
XAXIS	TIME
BEGINSTEP	1
ENDSTEP	10
BODY	PINION
SURFACE	FILLET1
TOOTHBEGIN	12
TOOTHEND	2
SEPTEETH	TRUE
SPROFBEGIN	0.00
SPROFEND	16.00
NUMSPROF	51
TFACEBEGIN	-1.00
TFACEEND	1.00
NUMTFACE	51
DEPTHBEGIN	0.00
DEPTHEND	0.00
NUMDEPTH	1
DISTMIN	0.05
OUTPUTTOFILE	TRUE
FILENAME	out.txt
APPEND	TRUE

2.2 Results and discussion

After the analysis is complete, a postprocessing data file is created in the working directory. A graph for the maximum principal normal stress against time for tooth numbers 12, 1 and 2 in the fillet region of the pinion obtained from the searchstress menu is shown in Figure 2.1.

The maximum stress in this case is $1.215 \times 10^5 psi$. The searchstress settings used to extract this graph is shown in Table 2.11.

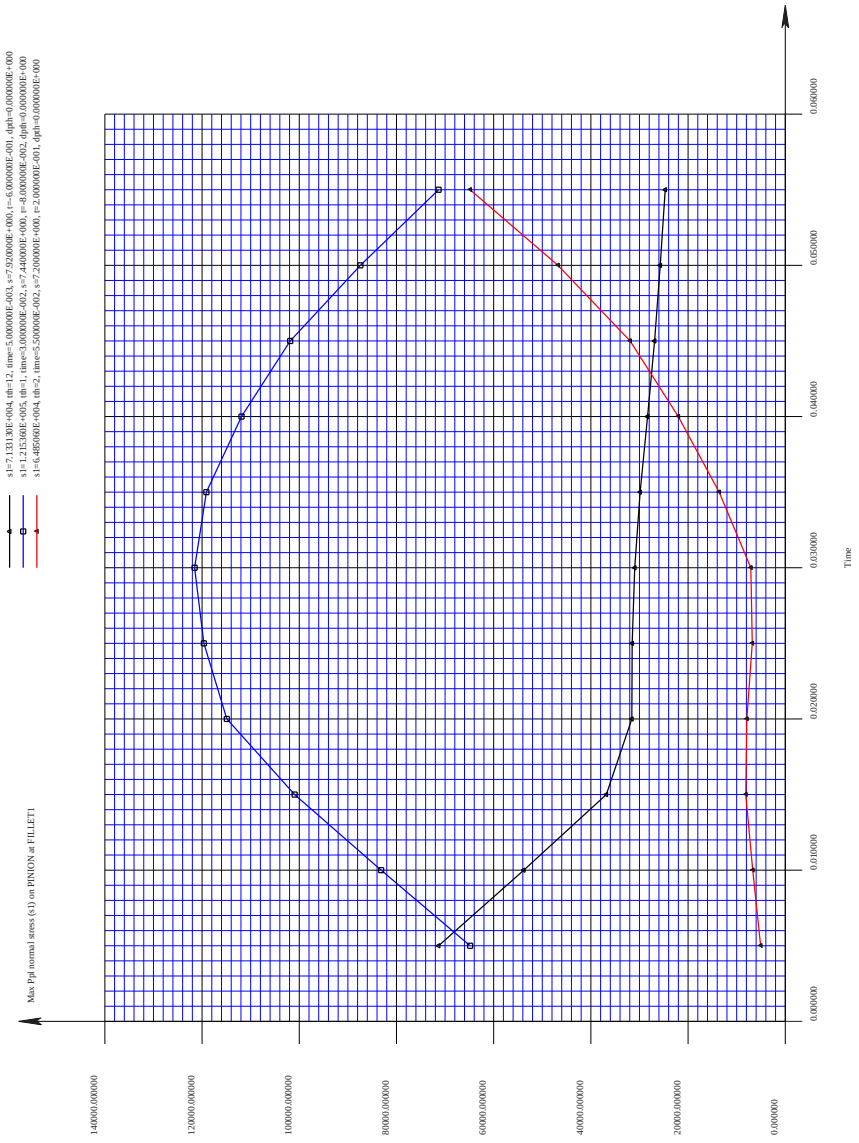

Figure 2.1: Graph of Max ppl normal stresses against time for a tip radius $0.045in$ with a medium template

Table 2.12: Max ppl normal stress values for different radii

Tip radius	Stress with medium.tpl	Stress with fineroot.tpl	Stress with finest.tpl
0.005	1.711E+05	1.892E+05	1.974E+05
0.01	1.638E+05	1.760E+05	1.812E+05
0.015	1.567E+05	1.661E+05	1.683E+05
0.02	1.500E+05	1.565E+05	1.581E+05
0.025	1.434E+05	1.482E+05	1.495E+05
0.03	1.370E+05	1.412E+05	1.421E+05
0.035	1.311E+05	1.351E+05	1.356E+05
0.04	1.259E+05	1.296E+05	1.299E+05
0.045	1.215E+05	1.266E+05	1.248E+05
0.05	1.192E+05	1.263E+05	1.224E+05
0.055	1.190E+05	1.260E+05	1.222E+05
0.06	1.187E+05	1.257E+05	1.220E+05
0.065	1.184E+05	1.254E+05	1.217E+05
0.07	1.174E+05	1.240E+05	1.205E+05
0.075	1.142E+05	1.208E+05	1.175E+05
0.08	1.099E+05	1.165E+05	1.133E+05
0.085	1.039E+05	1.104E+05	1.075E+05

2.2.1 Effect of Cutter Tip radius on the max ppl normal stress

In order to study the effect of cutter tip radius on the stress values we run the analysis for different tip radii for all the mesh templates. We vary the tip radius from $0.005in$ to $0.085in$ in steps of $0.005in$. The stress values obtained are shown in Table 2.12. Figure 2.2 shows a plot of Tip radius against the Max ppl normal stress. It can be concluded from the graph that as you go on increasing the tip radius, the stress decreases. From the graph it can be seen that the difference in the results for the medium and fineroot templates is 9.0% at a tip radius of $0.005in$. The difference in the results between fineroot and finest templates is about 4.0% at $0.005in$ tip radius. As expected, the agreement is better for larger values of tip radius.

Table 2.13 shows the results for the stresses over a much smaller range. The tip radius is varied from $0.04in$ to $0.045in$ in steps of $0.0005in$. Even for such a small change in tip radius, the change in stresses is monotonously decreasing.

The time required to run the analysis for each case with the medium, fineroot and finest templates was about $20mins$, $1hr$ and $4hrs$ respectively on an Intel $Pentium4$, $1700MHz$ *cpu*.

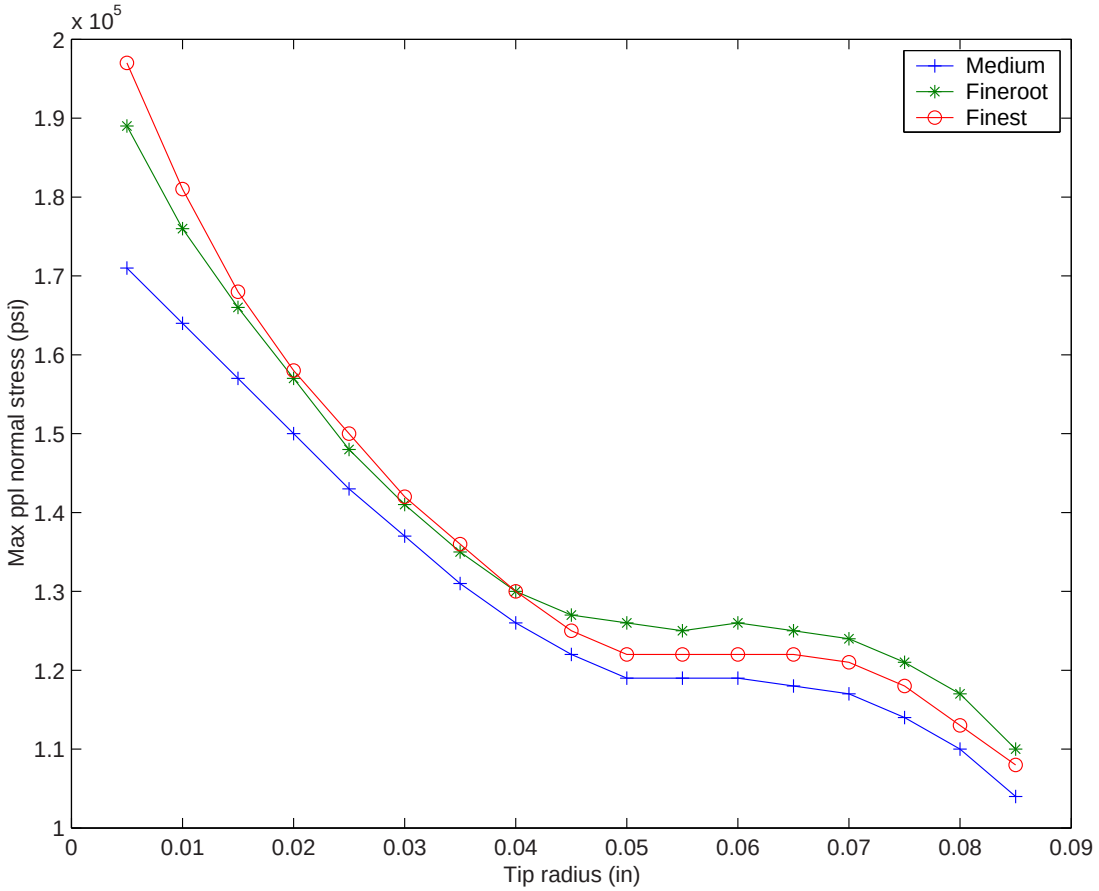

Figure 2.2: Graph of Max ppl normal stresses against tip radii ($0.005in - 0.085in$) for medium, fineroot and finest templates

Table 2.13: Max ppl normal stress values for different radii

Tip radius	Stress with medium.tpl
0.04	1.259E+05
0.0405	1.255E+05
0.041	1.250E+05
0.0415	1.245E+05
0.042	1.241E+05
0.0425	1.236E+05
0.043	1.232E+05
0.0435	1.228E+05
0.044	1.223E+05
0.0445	1.219E+05
0.045	1.215E+05

Table 2.14: Max ppl normal stress values for different tooth thicknesses

Tooth thickness	Stress with medium.tpl	Stress with fineroot.tpl	Stress with finest.tpl
0.32	1.215E5	1.266E5	1.248E5
0.315	1.231E5	1.263E5	1.261E5
0.31	1.248E5	1.290E5	1.270E5
0.305	1.273E5	1.313E5	1.289E5
0.3	1.294E5	1.330E5	1.312E5
0.295	1.313E5	1.349E5	1.340E5
0.29	1.342E5	1.375E5	1.364E5
0.285	1.366E5	1.396E5	1.381E5
0.28	1.385E5	1.412E5	1.394E5

2.2.2 Effect of Tooth thickness on the max ppl normal stress

In order to study the effect of tooth thickness on the stress values we run the analysis for different tooth thicknesses for all the mesh templates. We vary the thickness from $0.32in$ to $0.28in$ in steps of $0.005in$. The tip radius for all the tooth thickness values is $0.045in$. The stress values hence obtained are shown in Table 2.14. Figure 2.3 shows a plot of the Max ppl normal stress against tooth thickness. It can be concluded from the graph that as you go on decreasing the thickness, the stress increases. From the graph it can be seen that the difference in the results for the medium and fineroot templates is about 4.0%. The difference between the fineroot and finest templates is about 1.0%.

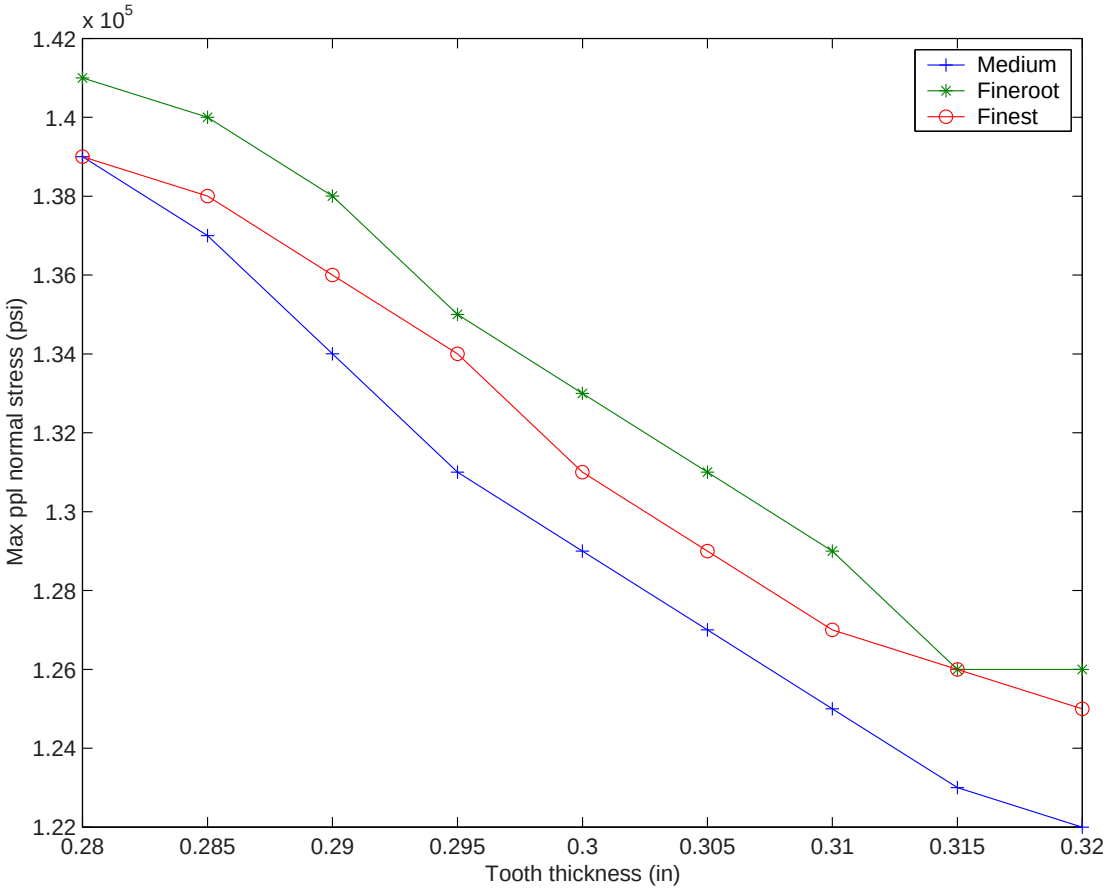

Figure 2.3: Graph of Max ppl normal stresses against tooth thickness (0.32in-0.28in) for medium, fineroot and finest templates

Table 2.15: Max ppl normal stress values for different number of elements along the face width

Nfaceelems	Stress with medium.tpl	Stress with fineroot.tpl	Stress with finest.tpl
2	1.207E5	1.239E5	1.242E5
4	1.215E5	1.266E5	1.248E5
6	1.212E5	1.243E5	-
8	1.211E5	1.243E5	-
10	1.211E5	1.242E5	-

2.2.3 Effect of number of elements in the face direction on the max ppl normal stress

In order to study the effect of number of elements along the face width on the stress values we run the analysis for different NFACEELEMS for all the mesh templates. We vary the NFACEELEMS parameter from 2 to 10 in steps of 2. The tip radius and the tooth thickness values for all the test cases are $0.045in$ and $0.32in$ respectively. The stress values hence obtained are shown in Table 2.15. Figure 2.4 shows a plot of the Max ppl normal stress against the no. of face elements for the medium and fineroot templates. Results for higher elements with the finest mesh could not be obtained due to CPU limitations. From the graph it can be seen that the difference in the results for the medium and fineroot templates is about 2.5%. As expected the stress values converge for higher number of elements.

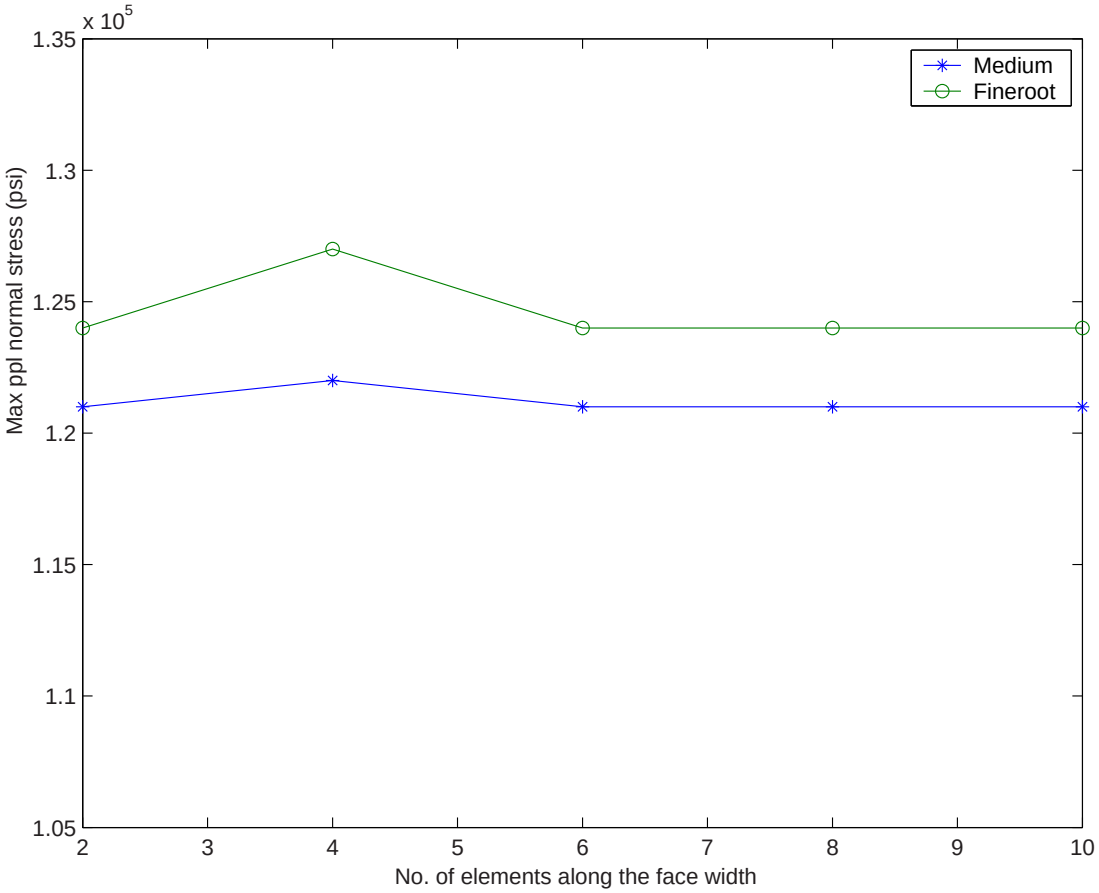

Figure 2.4: Graph of Max ppl normal stresses against No.of elements along the face width for medium and fineroot templates

Table 2.16: Max ppl normal stress values for different Displ. order

Displ.order	Stress with medium.tpl	Stress with fineroot.tpl	Stress with finest.tpl
3	1.215E5	1.266E5	1.248E5
4	1.211E5	1.243E5	-
5	1.211E5	1.242E5	-
6	1.211E5	1.242E5	-

2.2.4 Effect of displacement order on the max ppl normal stress

In order to study the effect of the displacement order on the stress values we run the analysis for different DISPLORDER for all the mesh templates. With 4 elements along the face width, we vary the DISPLORDER parameter from 3 to 6 in steps of 1. The tip radius and the tooth thickness values for all the test cases are $0.045in$ and $0.32in$ respectively. The stress values hence obtained are shown in Table 2.16. Figure 2.5 shows a plot of the Max ppl normal stress against the displ. order for the medium and fineroot templates. Results for higher order with the finest mesh could not be obtained due to CPU limitations. From the graph it can be seen that the difference in the results for the medium and fineroot templates is about 4.0%. The results converge for higher order as expected.

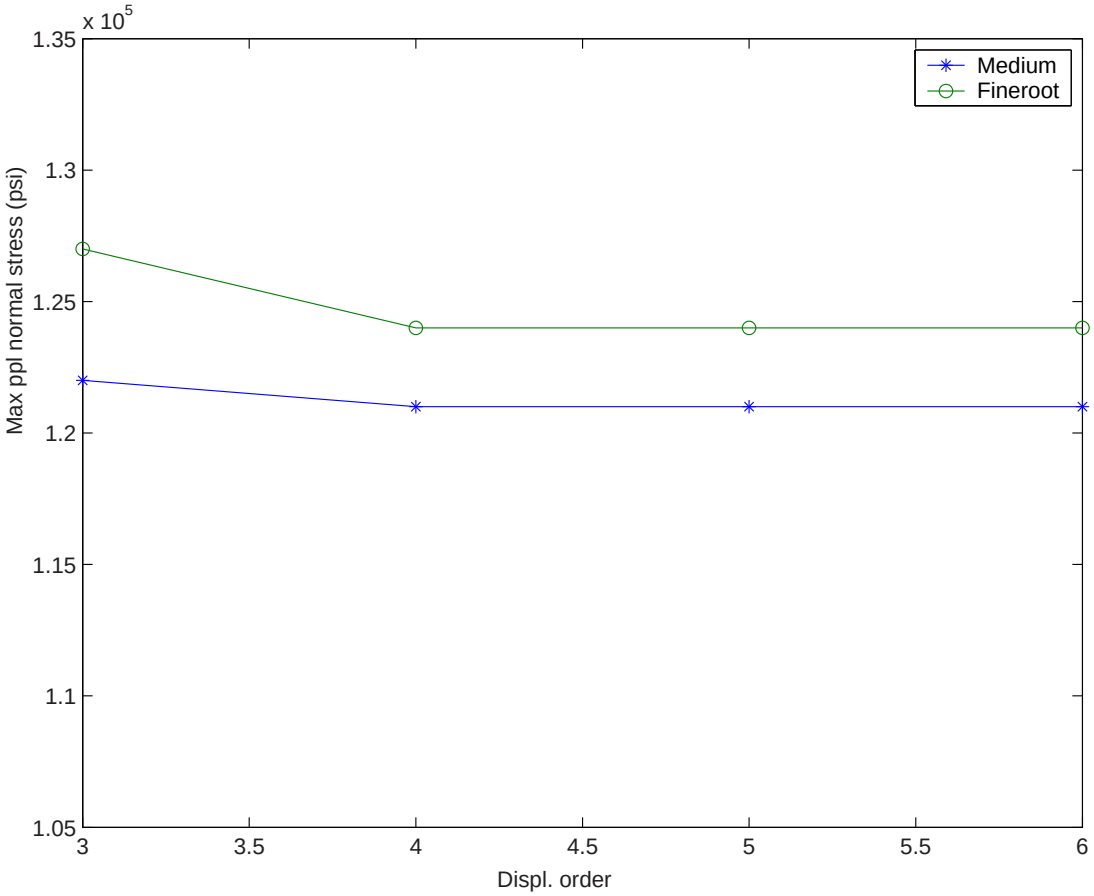

Figure 2.5: Graph of Max ppl normal stresses against displ. order for medium and fineroot templates

2.3 Conclusions

The stress values have been shown to converge with increasing refinement of the finite element mesh. For typical tip radius values, this convergence study shows that we have a discretization error of about 4.0% in the coarsest mesh (medium.tpl) and less than 1.0% in the intermediate mesh (fineroot.tpl). We feel that the error in the finest mesh (finest.tpl) is much less than 1.0%. The stress values converge with higher elements along the face direction and also with a higher order fourier series. The error in the results for less number of face elements and less displ. order is about 4.0% for the medium template and less than 1.0% for the fineroot template.

Chapter 3

Fatigue theory and life prediction using the hypoid gear program

3.1 Introduction

Most engineering design projects involve machine parts subjected to fluctuating or cyclic loads. Such loading induces fluctuating or cyclic stresses that often result in failure by fatigue. Materials fracturing under repeated loadings are found to exhibit no gross deformation and give the appearance of having suddenly snapped. It is difficult to detect the progressive changes in the material properties that occur during fatigue stressing and failure may therefore occur with little or no warning. Also, periods of rest, with the fatigue stress removed, do not lead to any measurable healing or recovery from the effects of prior cyclic stressing. Thus the damage done during the fatigue process is cumulative and generally unrecoverable.

Fatigue is by far the most common cause of failure of load carrying metallic parts operating at or close to room temperature.

3.2 Fatigue characteristics

Fatigue may be characterised as a progressive failure phenomenon that proceeds by the initiation and propagation of cracks to an unstable size. Fatigue crack nuclei, from which cracks grow and often propagate to failure, are thought to be formed through the movements of dislocations that produce fine slip bands at the crystal surfaces. Under cyclic loading these fine slip bands ultimately turn out to be the regions in which fatigue cracks are initiated. Further, the fatigue slip bands gives rise to intrusions as a result of reversed slip in adjacent slip planes caused by load reversal. Once formed, these intrusions grow in depth by reverse slip process, and their growth may well constitute a major portion of the fatigue of the metal. Crack propagation and hence fatigue are affected by various factors such as material composition, grain size and grain direction, heat treatment, welding, geometrical discontinuities, surface conditions, size, residual surface stresses, corrosion, fretting, operating temperature, operating speed, etc.

A term called fatigue limit(endurance limit) is very commonly used while studying fatigue failure. It is the stress level below which an infinite number of cycles can be sustained without failure. To characterize the failure response of components in the finite life range, the term fatigue strength at a specified life, S_N is used. The term fatigue strength identifies the stress level at which failure will occur at specified life.

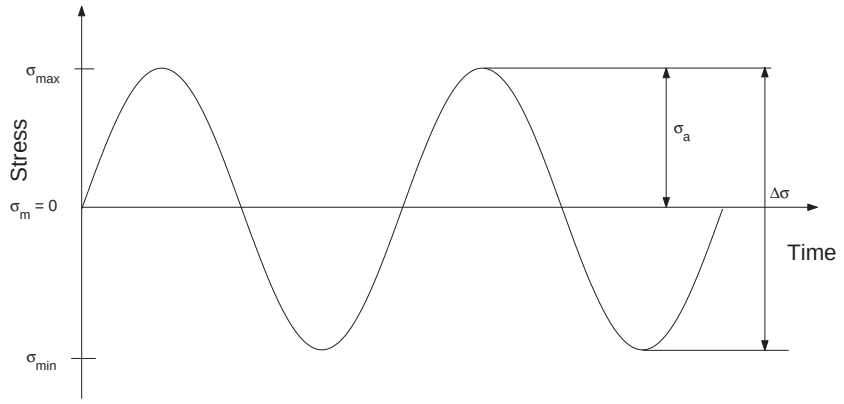

Figure 3.1: Completely reversed cyclic stress plot

3.3 Low and High cycle fatigue

It is observed that the fatigue process embraces two domains of cyclic stressing or straining that are significantly different in character, and in each of which failure is probably produced by different physical mechanisms. One domain of cyclic loading is that for which significant plastic strains occur during each cycle. This domain is associated with high loads and short lives, or low number of cycles to produce fatigue failure, and is commonly referred to as low cycle fatigue.

The other domain of cyclic loading is that for which the strain cycles are largely confined to the elastic range. This domain is associated with lower loads and long lives, or high number of cycles to produce fatigue failure, and is commonly referred to as high cycle fatigue. Low-cycle fatigue is typically associated with cycle lives up to about 10^4 or 10^5 cycles, and high cycle fatigue for lives greater than about 10^4 or 10^5 cycles. In most gearing applications fatigue failure is associated with high cycle fatigue. Hence we address the hypoid fatigue failure problem based on the theory related to the high cycle fatigue.

3.4 Fatigue loading

As discussed earlier fatigue failure is caused in materials or components when subjected to cyclic or alternating stress. A simple example of a fatigue stress spectrum to which an element may be subjected could be a zero-mean sinusoidal stress-time pattern of constant amplitude and fixed frequency, applied for a specified number of cycles. Such a stress-time pattern, often referred to as a completely reversed cyclic stress is shown in Figure 3.1.

Using the figure we define the following terms and symbols so as to calculate the fatigue strength or fatigue life for a hypoid gear set.

$$\sigma_{max} = \text{Maximum Stress in the cycle} \tag{3.1}$$

$$\sigma_{min} = \text{Minimum Stress in the cycle} \tag{3.2}$$

$$\sigma_m = \text{Mean Stress} = \frac{\sigma_{max} + \sigma_{min}}{2} \tag{3.3}$$

$$\sigma_a = \text{Alternating Stress amplitude} = \frac{\sigma_{max} - \sigma_{min}}{2} \tag{3.4}$$

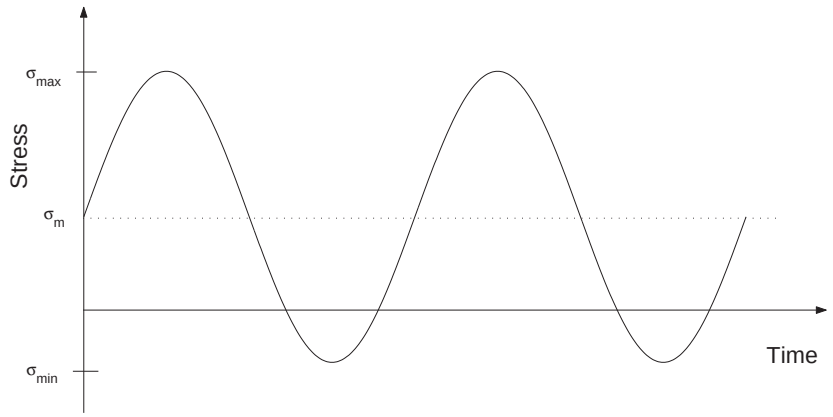

Figure 3.2: Nonzero mean stress-time pattern

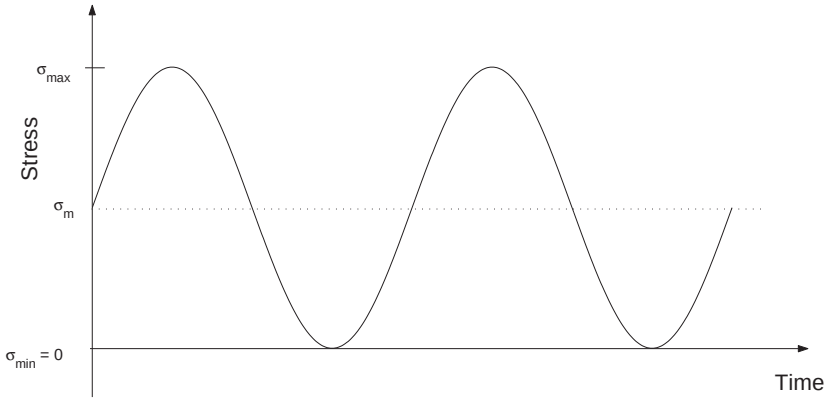

Figure 3.3: Released tension, R=0, stress-time pattern

$$\begin{aligned} \Delta\sigma &= \text{Range of Stress} \\ &= \sigma_{max} - \sigma_{min} \qquad (3.5) \\ R &= \text{Stress Ratio} \\ &= \frac{\sigma_{min}}{\sigma_{max}} \qquad (3.6) \\ A &= \text{Amplitude Ratio} \\ &= \frac{\sigma_a}{\sigma_m} \qquad (3.7) \end{aligned}$$

Some examples of other Stress-time patterns are shown in Figures 3.2 through 3.7.

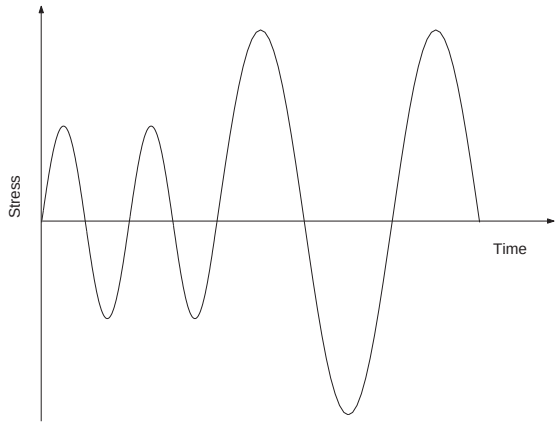

Figure 3.4: Changing amplitude stress-time pattern

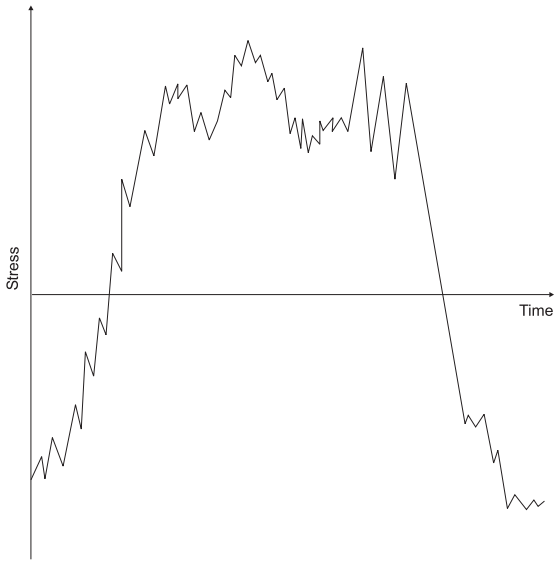

Figure 3.5: Quasi-random stress-time pattern

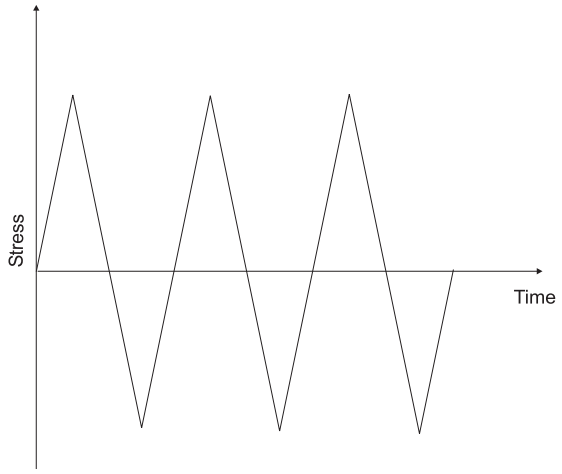

Figure 3.6: Completely reversed ramp stress-time pattern

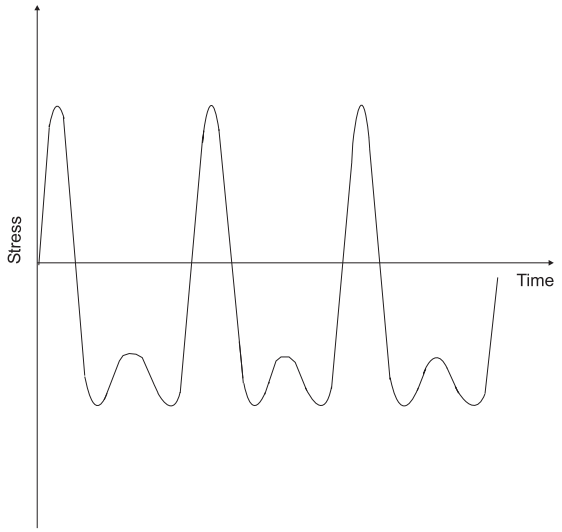

Figure 3.7: Stress-time pattern with distorted peaks

3.5 Example of a laboratory fatigue testing

Designing machine parts or structures that are subjected to fatigue loading is usually based on the results of laboratory fatigue tests using specimens of the material of interest. An example of a laboratory fatigue test called the rotating bending machine of the constant bending moment type is shown in Figure 3.8.

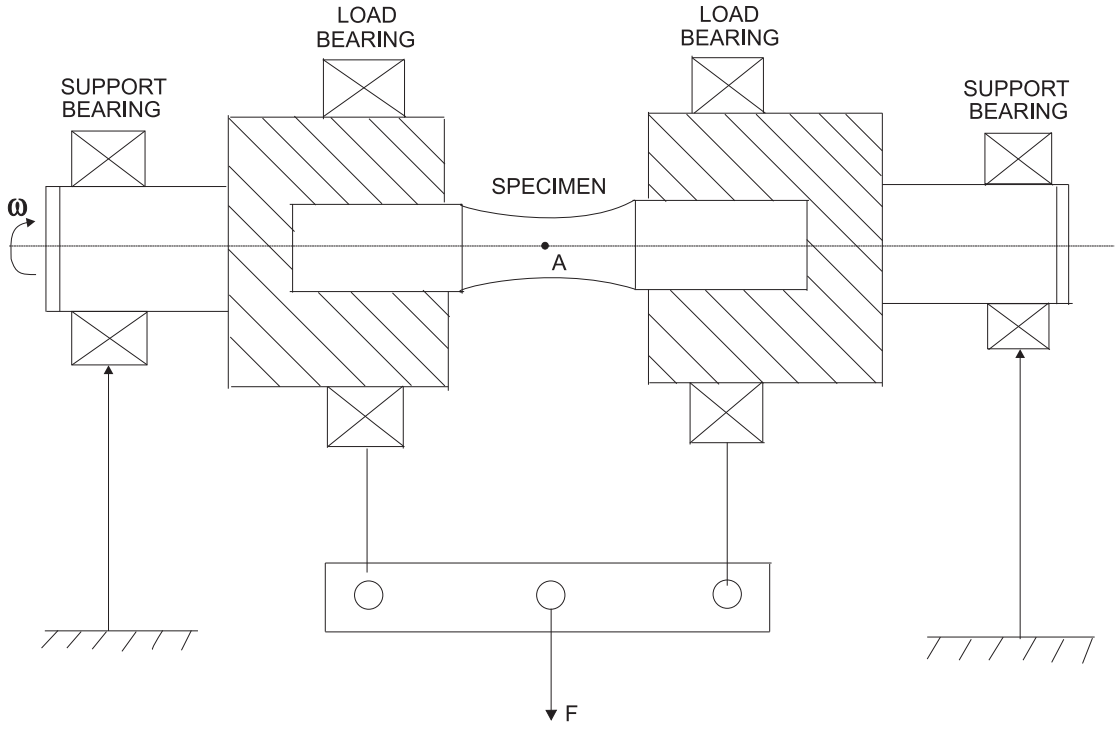

Figure 3.8: Schematic of the rotating-bending fatigue testing machine of the constant bending moment type

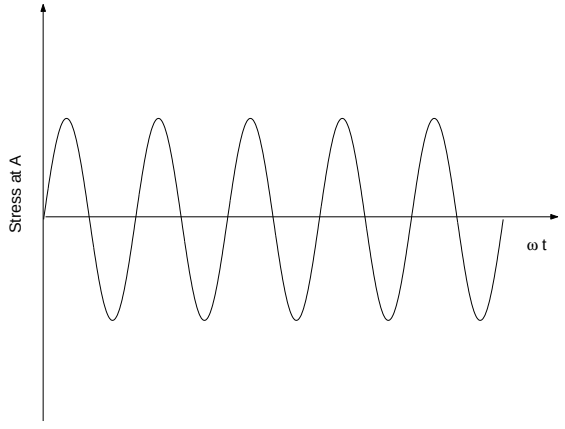

Figure 3.9: Stress-time pattern for point A at the surface of the critical section

With this type of device the region of the rotating beam between the inboard bearings is subjected to a constant bending moment all along its length. While under the influence of this constant moment, the specimen is rotated with the drive spindles about its longitudinal axis. Any point on the surface is thereby subjected to a completely reversed stress-time pattern, as can be deduced by following the stress history of a point as it rotates from maximum compression at the top position down through zero stress when at the side through maximum tension at the bottom, and then back through zero to maximum compression at the top again. The stress-time pattern for a point on the surface of the critical section is shown in Figure 3.9.

3.6 Gear fatigue failure

Gears may fail by wear and scuffing but the main causes of failure are bending fatigue leading to breakage at the root of the tooth and surface contact fatigue leading to pitting. Fatigue failure in gears can be broadly classified in to two types:

- Those arising from a **tensile fatigue** failure of the material at the root of a gear tooth i.e. away from the area of contact between intermeshing teeth.
- Those arising from **compressive stresses** on the working surface of the gear tooth, where it is in contact with the intermeshing gear.

Tensile fatigue failure occurs in materials subjected to fluctuating stresses where the continuously repeated stress is much lower than the static tensile strength of the material. This type of high cycle fatigue failure generally depends upon the number of stress cycles rather than on the total time under load and does not occur below a certain stress, called the fatigue and endurance limit. In a homogeneous material tensile fatigue crack always starts at and propagates from the point of maximum stress concentration. Under normal operation and with correct design the point of maximum tensile stress concentration on a gear is at the root of the tooth on the loaded side. The crack progresses through the tooth to the root on the opposite side. During this crack propagation the tooth can bend over and shed the load on to the next tooth which also ultimately fails.

Surface fatigue failure is brought about by cumulative damage to the gear material caused by repeated application of contact stresses. Surface contact fatigue does not usually lead to catastrophic breakage (as in the case of a tensile fatigue failure) but rather to progressive deterioration of the surface by pitting or spalling.

3.7 Running the Hypoid facemilled program for fatigue failure

3.7.1 The example file

Load the file `fatigue.ses` from the `FATIGUE` directory located in the `SAMPLES` directory.

The data for the fatigue test model is similar to the data we used for convergence study. We run the analysis for one mesh cycle.

3.7.2 Locating the point of maximum stress

The SEARCHSTRESS menu is used to locate the point of maximum stress on the profile, facewidth and the depth of a tooth. A plot of maximum principal stress against time for Pinion tooth no.1 is shown in Figure 3.10. The legend on the top right corner of the figure shows the location along the profile(s), width(t) and the depth(dpth) of the maximum stress point. The search stress menu used to plot this graph is shown in Table 3.1. The depth on the surface of the tooth is 0.00. As can be seen from the stress results the maximum stress occurs at profile, $s = 7.56$. The involute profile as shown in Figure 3.11 goes from $s = 0$ to $s = 48$. There are 8 elements along the profile(element nos.3 through 10). So each element corresponds to a profile distance of 6 units. From figure 3.11 and figure 3.12 the point of maximum stress lies between the profile, $s = 6$ and $s = 12$. To find the corresponding XI(ξ) co-ordinate we use the following:

$$\begin{aligned} \frac{\xi - (-1)}{2} &= \frac{7.56 - 12}{6 - 12} \\ \xi &= 0.48 \end{aligned} \tag{3.8}$$

The ETA(η) co-ordinate on the surface is 1.00.

Since there are 4 finite elements along the width and the point of maximum stress lies close to 0.00($t = -0.08$) we are interested in element numbers 40 and 76. The element orientation is shown in Figure 3.12. Refer to the appendix of the Hypoid Facemilled Users manual for further details. Note that ZETA(ζ) is along the facewidth direction. So as to locate the exact ζ value we apply FEPROBES close to $\zeta = +1$ for element no.40 and $\zeta = -1$ for element no.76. The FE probe menu for one of the probes is shown in table 3.2. Analysing the FE probe data the co-ordinates of the maximum stress point is found to be (ξ, η, ζ) = (0.48, 1.00, 0.66) on element no.40. For this point the plot of maximum and minimum principal normal stress against time is shown in Figure 3.13.

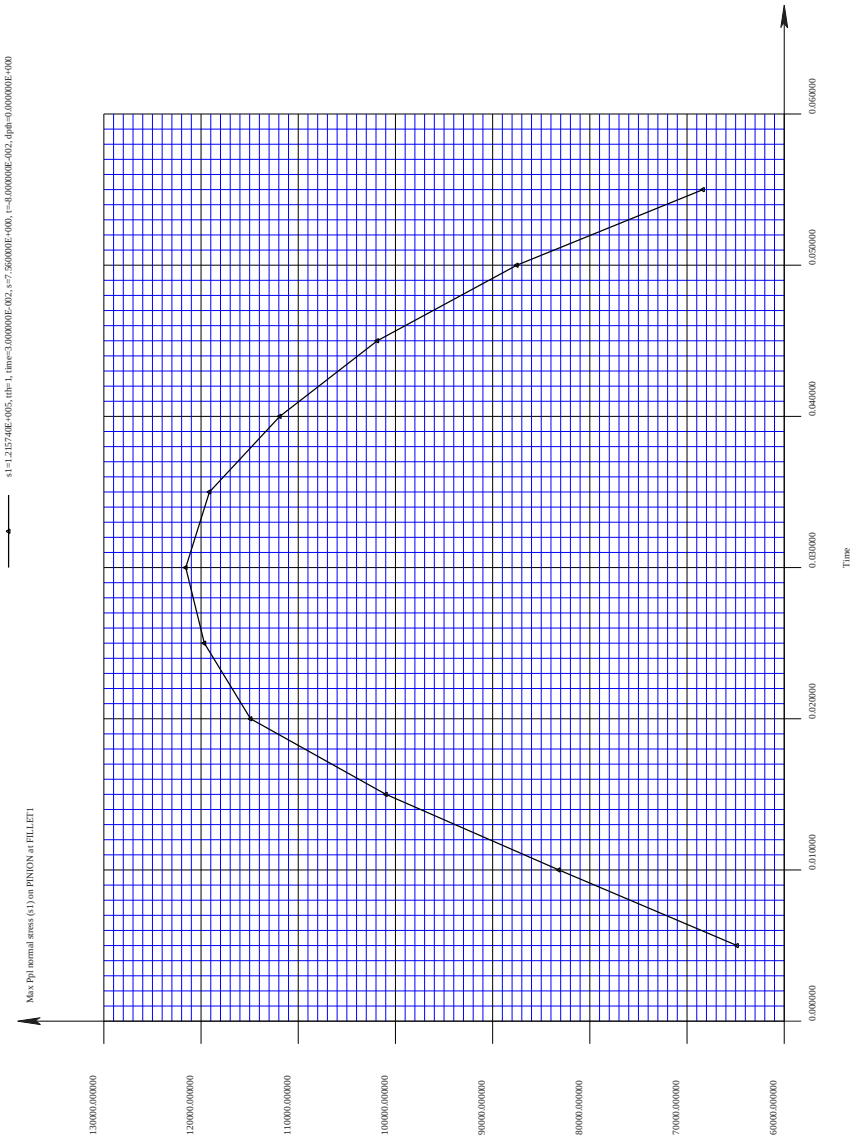

Figure 3.10: Plot of maximum principal normal stress against time for pinion tooth no.1 using the SEARCHSTRESS menu

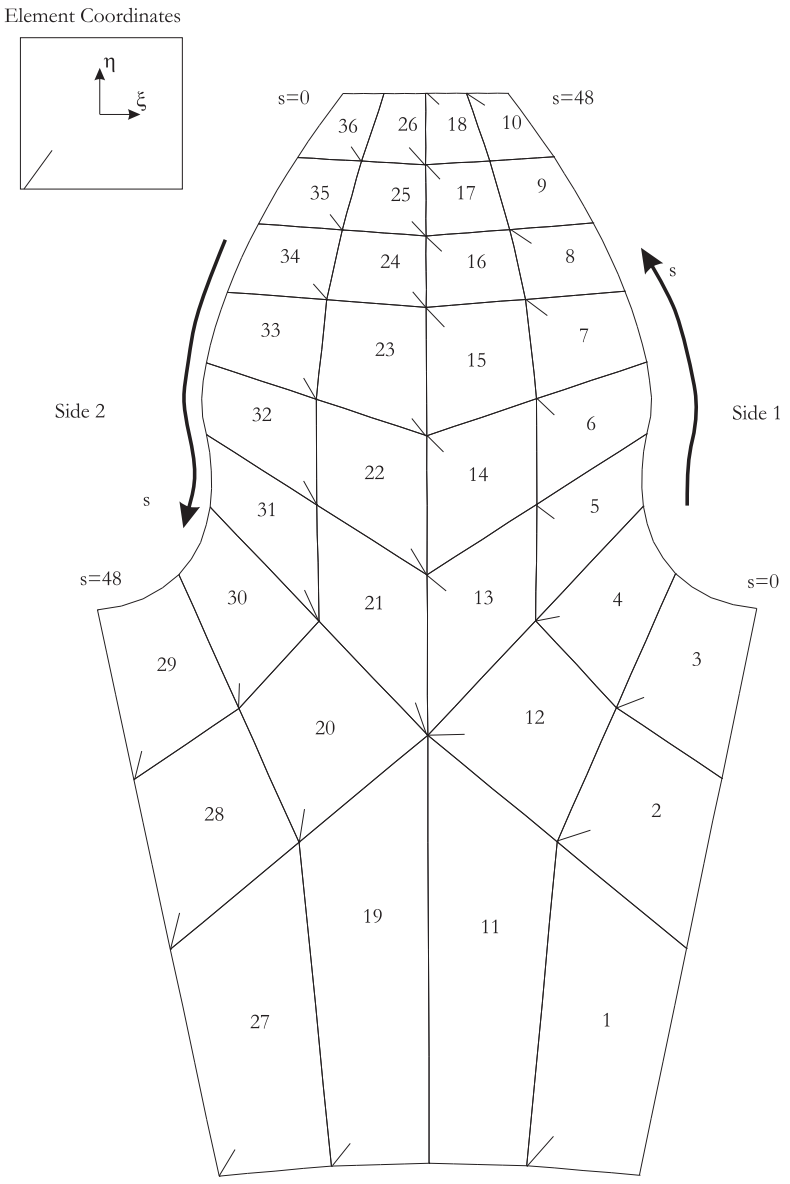

Figure 3.11: The MEDIUM.TPL template file.

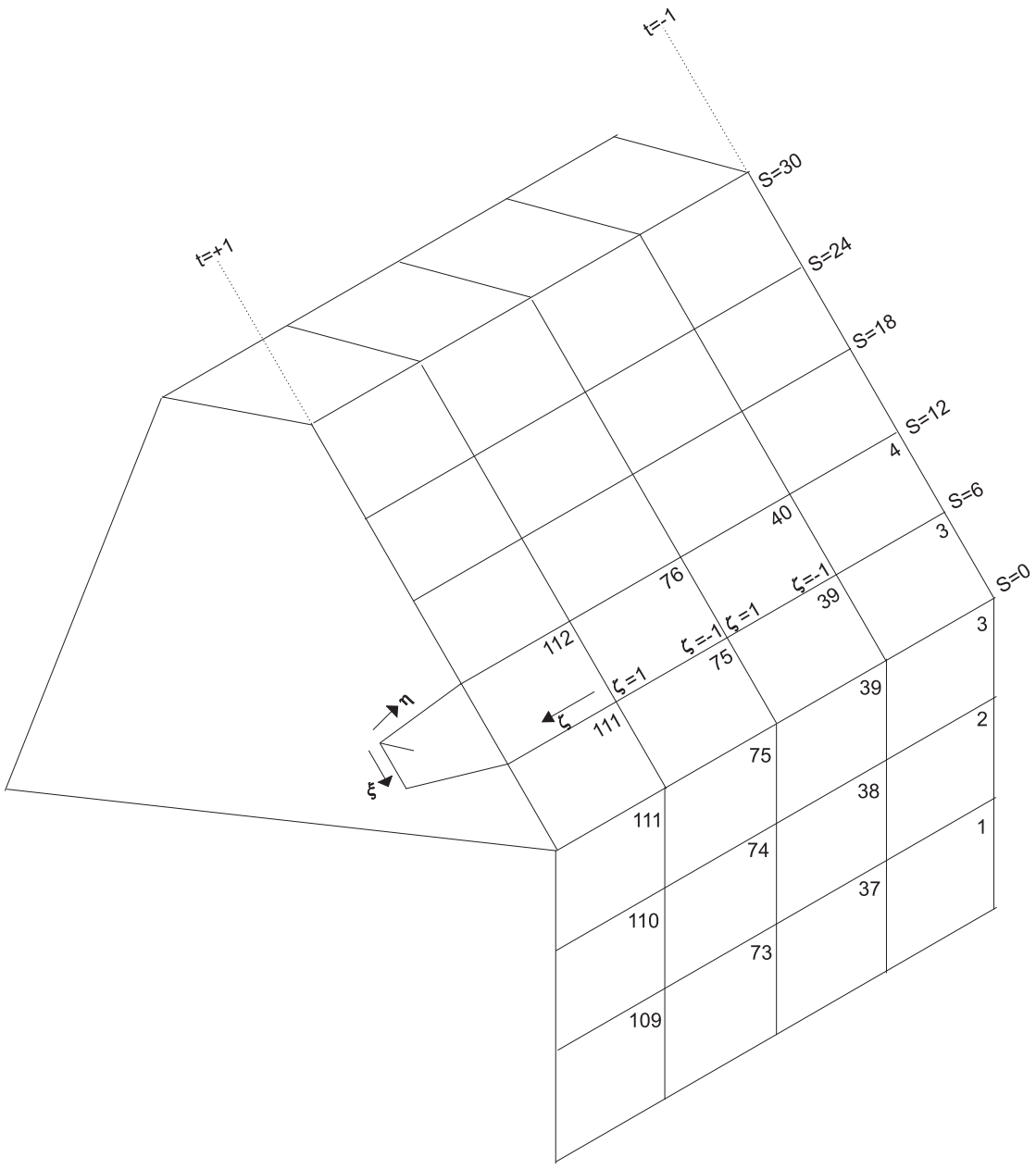

Figure 3.12: Orientation of ξ, η and ζ on the tooth

Table 3.1: Searchstress data

Item	Description
COMPONENT	MAXPPLSTRESS
XAXIS	TIME
BEGINSTEP	1
ENDSTEP	11
BODY	PINION
SURFACE	FILLET1
TOOTHBEGIN	1
TOOTHEND	1
SEPTEETH	TRUE
SPROFBEGIN	6.00
SPROFEND	12.00
NUMSPROF	51
TFACEBEGIN	-0.5
TFACEEND	0.5
NUMTFACE	51
DEPTHBEGIN	0.00
DEPTHEND	0.00
NUMDEPTH	1
DISTMIN	0.05
OUTPUTTOFILE	TRUE
FILENAME	out.txt
APPEND	TRUE

Table 3.2: FE probe data

Item	Description
NPROBES	40
PROBE	1
BODY	PINION
MESH	TOOTH
ELEM	40
XI	0.48
ETA	1.00
ZETA	0.66
COMPONENT	MAXPPLNORMAL
FILENAME	PROBES.DAT

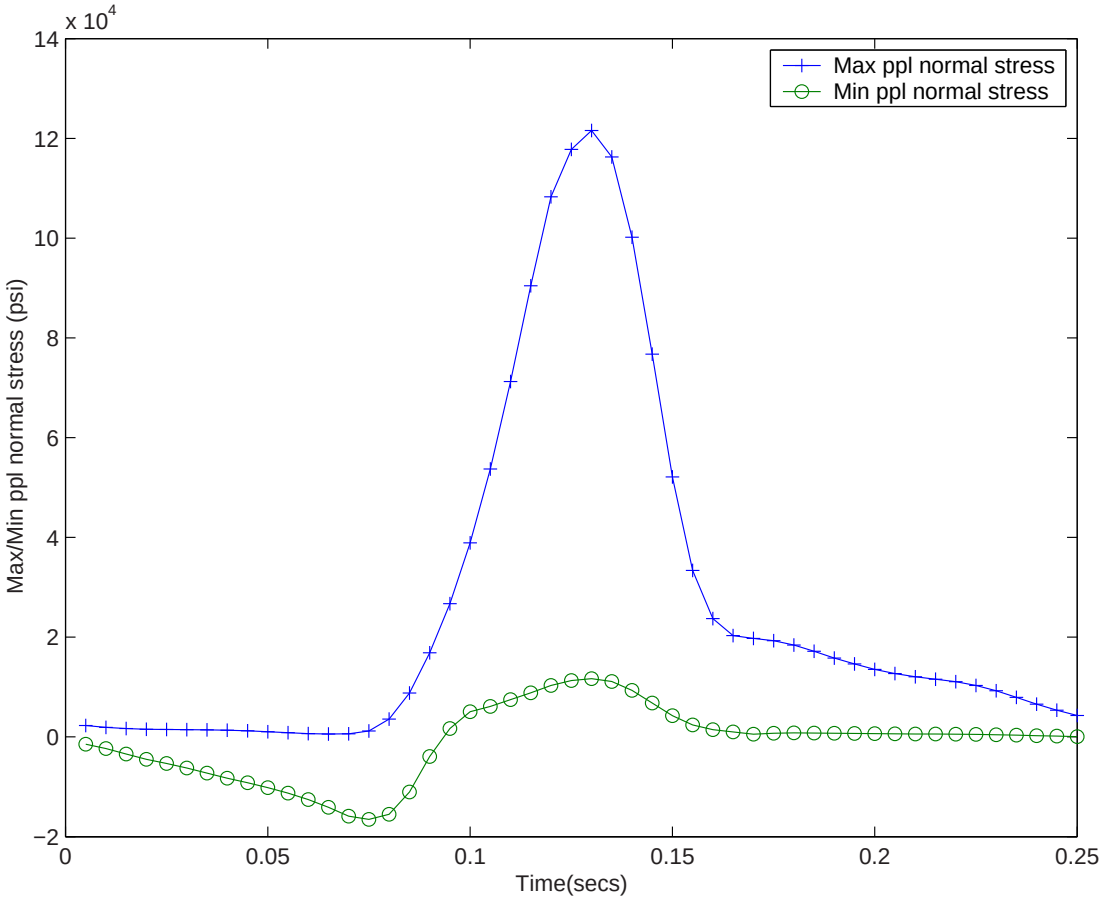

Figure 3.13: Plot of maximum and minimum principal normal stress for a point on the pinion tooth against time

3.7.3 Results

The maximum principal and the minimum principal normal stress plot obtained from the FE probe data is shown in Figure 3.13. The maximum principal normal stress ($\sigma_{\max}$) = $1.21574 \times 10^5 psi$ and the minimum principal normal stress ($\sigma_{\min}$) = $-1.655067 \times 10^4 psi$. Hence, Alternating stress, $\sigma_{\mathrm{a}} = 6.90623 \times 10^4 psi$ and the Mean stress, $\sigma_{\mathrm{m}} = 5.25116 \times 10^4 psi$.

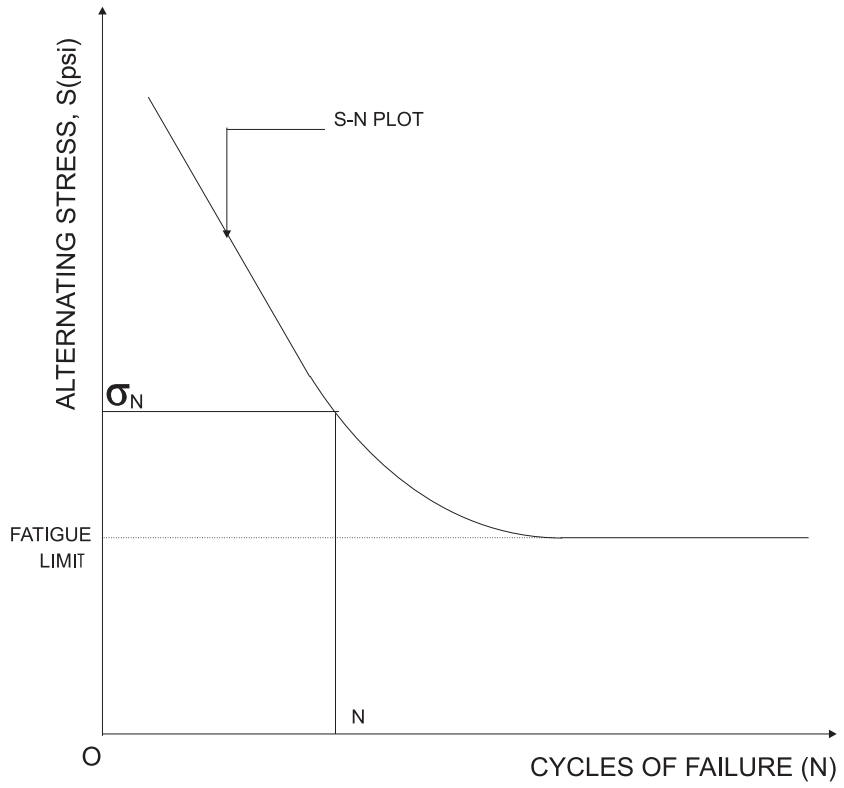

Figure 3.14: An example of an S-N curve for predicting fatigue life

3.8 Calculating the fatigue life

The stress life, S-N, method was the first approach used in an attempt to understand and quantify fatigue life. The S-N approach is still widely used in design applications where the applied stress is primarily within the elastic range of the material and the resultant lives (cycles to failures) are long, such as power transmission shafts. The S-N diagram is a plot of alternating stress, S, versus cycles to failure, N. One of the major drawbacks of the stress-life approach is that it ignores the true stress-strain behavior and treats all strains as elastic. This may be significant since the initiation of fatigue cracks is caused by plastic deformation. The simplifying assumptions of the S-N approach are valid only if the plastic strains are small. At long lives most steels have only a small component of cyclic strain which is plastic and the S-N approach is valid. An example of an S-N plot is shown in Figure 3.14.

The magnitude of mean stress has an important influence on the fatigue behavior of a specimen or a machine part. Most service applications involve nonzero mean cyclic stresses. The present case under consideration also is an example of a nonzero mean cyclic stress. The influence of non-zero mean stress on failure can be estimated by empirical relationships (Figure 3.15) that relate the failure at a given life under non-zero mean conditions to failure at the same life under zero mean cyclic stresses.

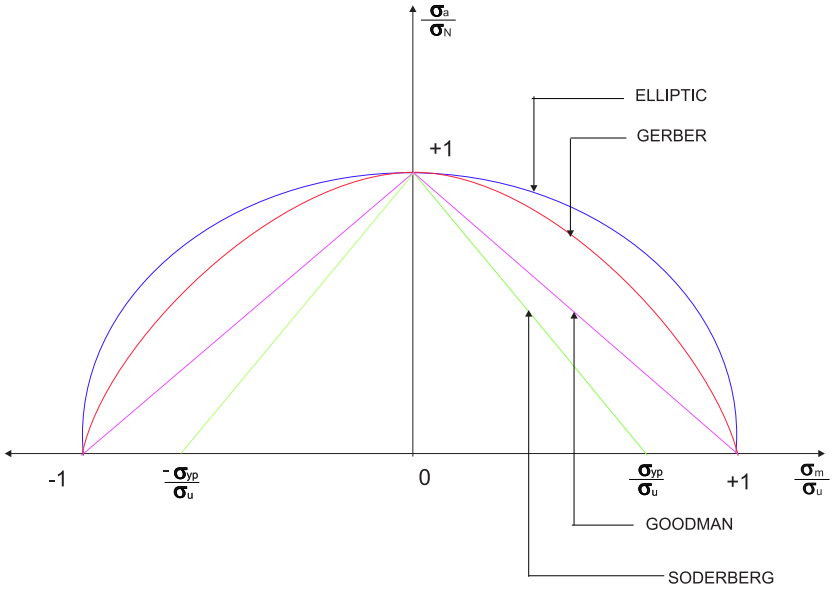

Figure 3.15: Various empirical relationships for estimating the influence of nonzero-mean stress on fatigue failure

3.8.1 Goodman's Linear relationship

Let,

$$\begin{aligned} \sigma_a &= \text{Alternating stress amplitude} \\ \sigma_N &= \text{Fatigue strength} \\ \sigma_m &= \text{Mean stress} \\ \sigma_u &= \text{Ultimate strength} \\ \sigma_{y_p} &= \text{Yield point stress} \end{aligned}$$

`Goodman's linear relationship` states that fatigue failure occurs when

$$\frac{\sigma_a}{\sigma_N} + \frac{\sigma_m}{\sigma_u} \geq 1 \tag{3.9}$$

For G43400 steel [1] with tensile strength $180kpsi$ and fatigue limit $120kpsi$, using the results for σ_a and σ_m, the Goodman linear relationship gives

$$\frac{\sigma_a}{\sigma_N} + \frac{\sigma_m}{\sigma_u} = 0.8672$$

[1] See 'Mechanical Engineering Design', Fourth Edition, Shigley and Mitchell, pages 276-277

3.8.2 Gerber's parabolic relationship

`Gerber's parabolic relationship` states that fatigue failure occurs when

$$\frac{\sigma_a}{\sigma_N} + (\frac{\sigma_m}{\sigma_u})^2 \quad \geq \quad 1 \tag{3.10}$$

For G43400 steel with tensile strength $180kpsi$ and fatigue limit $120kpsi$, the Gerber's parabolic relationship gives

$$\frac{\sigma_a}{\sigma_N} + (\frac{\sigma_m}{\sigma_u})^2 \quad = \quad 0.66$$

3.8.3 Soderberg's linear relationship

`Soderberg's linear relationship` states that fatigue failure occurs when

$$\frac{\sigma_a}{\sigma_N} + \frac{\sigma_m}{\sigma_{y_p}} \quad \geq \quad 1 \tag{3.11}$$

For G43400 steel with yield strength $160kpsi$ and fatigue limit $120kpsi$, the Soderberg's linear relationship gives

$$\frac{\sigma_a}{\sigma_N} + \frac{\sigma_m}{\sigma_{y_p}} \quad = \quad 0.9031$$

3.8.4 Elliptic relationship

`Elliptic relationship` states that fatigue failure occurs when

$$(\frac{\sigma_a}{\sigma_N})^2 + (\frac{\sigma_m}{\sigma_u})^2 \quad \geq \quad 1 \tag{3.12}$$

For G43400 steel with tensile strength $140kpsi$ and fatigue limit $71kpsi$, the Elliptic relationship gives

$$(\frac{\sigma_a}{\sigma_N})^2 + (\frac{\sigma_m}{\sigma_u})^2 \quad = \quad 0.4153$$

The above theories can be used to find the alternating stress at which fatigue failure will occur. For instance, according to the Goodman's linear relationship, for a steel with tensile strength $180kpsi$, the fatigue stress can be calculated by substituting $\sigma_a = 6.90623 \times 10^4 psi$, $\sigma_m = 5.25116 \times 10^4 psi$ and $\sigma_u = 180 \times 10^3 psi$ in to Goodman linear relationship giving $\sigma_N = 97.5081 \times 10^3 psi$. Using an S-N plot for steel shown in Figure 3.16 [2], the corresponding fatigue life is $4.4 \times 10^5 cycles$. Note that the S-N plot used in the figure is not a standard curve for gear materials. It is used to demonstrate the ability of the hypoid facemilled program in calculating the fatigue life.

[2] See 'Fundamentals of metal fatigue analysis', Prentice Hall, Bannantine, Comer, Handrock, pages 1-5

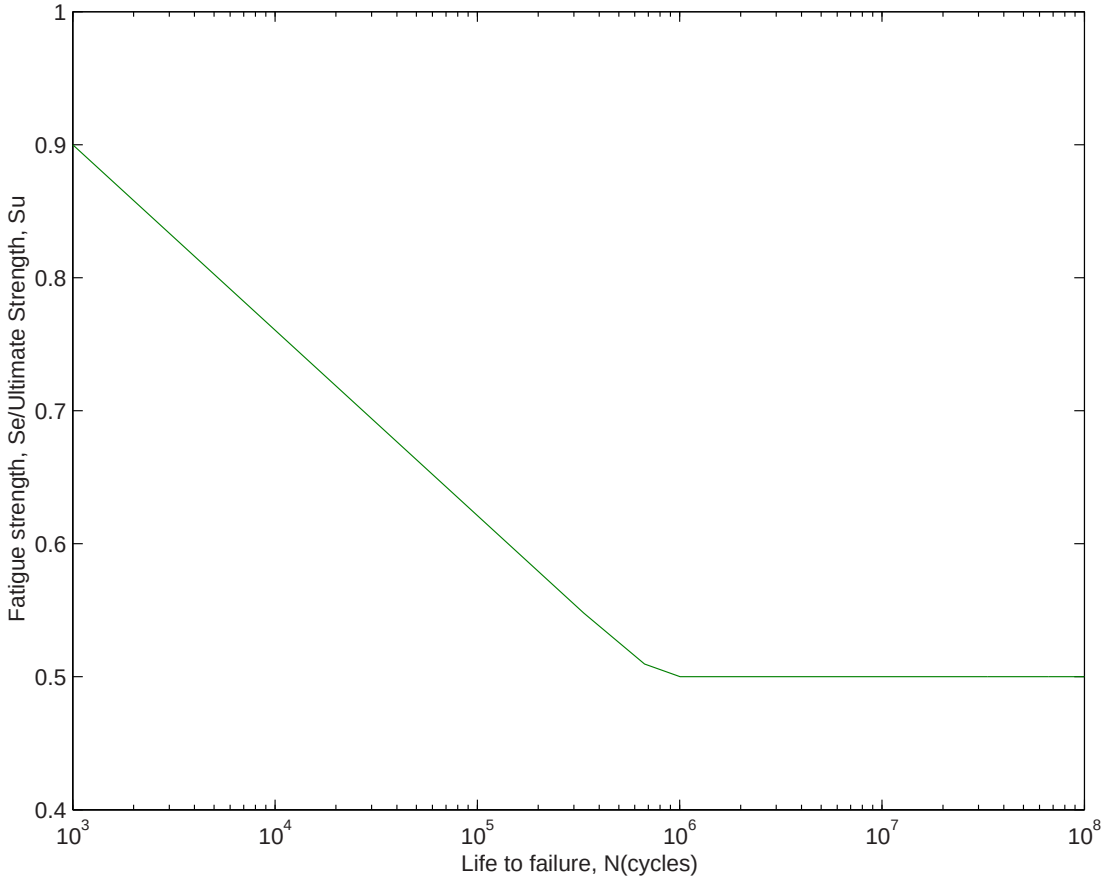

Figure 3.16: Example of an S-N plot for wrought steel

3.9 Effect of rigid internal diameter on fatigue life

In order to study the effect of the boundary condition on fatigue life we make the inner diameter of the pinion as rigid. Load the file `fatigueinnerdiarigid.ses` located in the `FATIGUE` directory. The ISRACERIGID item in the COMMON menu data for the pinion is turned on to make the inner diameter of the pinion as rigid.

3.9.1 Locating the point of maximum stress

The SEARCHSTRESS menu is used to locate the point of maximum stress on the profile, facewidth and the depth of a tooth. A plot of maximum principal stress against time for Pinion tooth no.1 is shown in Figure 3.17. The legend on the top right corner of the figure shows the profile(s), width(t) and the depth(dpth) data of the maximum stress point. The search stress menu used to plot this graph is shown in Table 3.3. The depth on the surface of the tooth is 0.00. As can be seen from the stress results the maximum stress occurs at profile, $s = 7.70$. Thus the point of maximum stress lies between the profile, $s = 6$ and $s = 12$. To find the corresponding XI(ξ) co-ordinate we use the following:

$$\begin{aligned} \frac{\xi - (-1)}{2} &= \frac{7.70 - 12}{6 - 12} \\ \xi &= 0.433 \end{aligned} \tag{3.13}$$

The ETA(η) co-ordinate on the surface is 1.00.

Since there are 4 finite elements along the width and the point of maximum stress lies close to 0.00($t = -0.08$) we are interested in element numbers 40 and 76. Refer to the appendix of the Hypoid Facemilled Users manual for further details. So as to locate the exact ζ value we apply FEPROBES close to $\zeta = +1$ for element no.40 and $\zeta = -1$ for element no.76. The FE probe menu for one of the probes is shown in table 3.4. Analysing the FE probe data the co-ordinates of the maximum stress point is found to be (ξ, η, ζ) = (0.433, 1.00, 0.68) on element no.40. For this point the plot of maximum and minimum principal normal stress against time is shown in Figure 3.18.

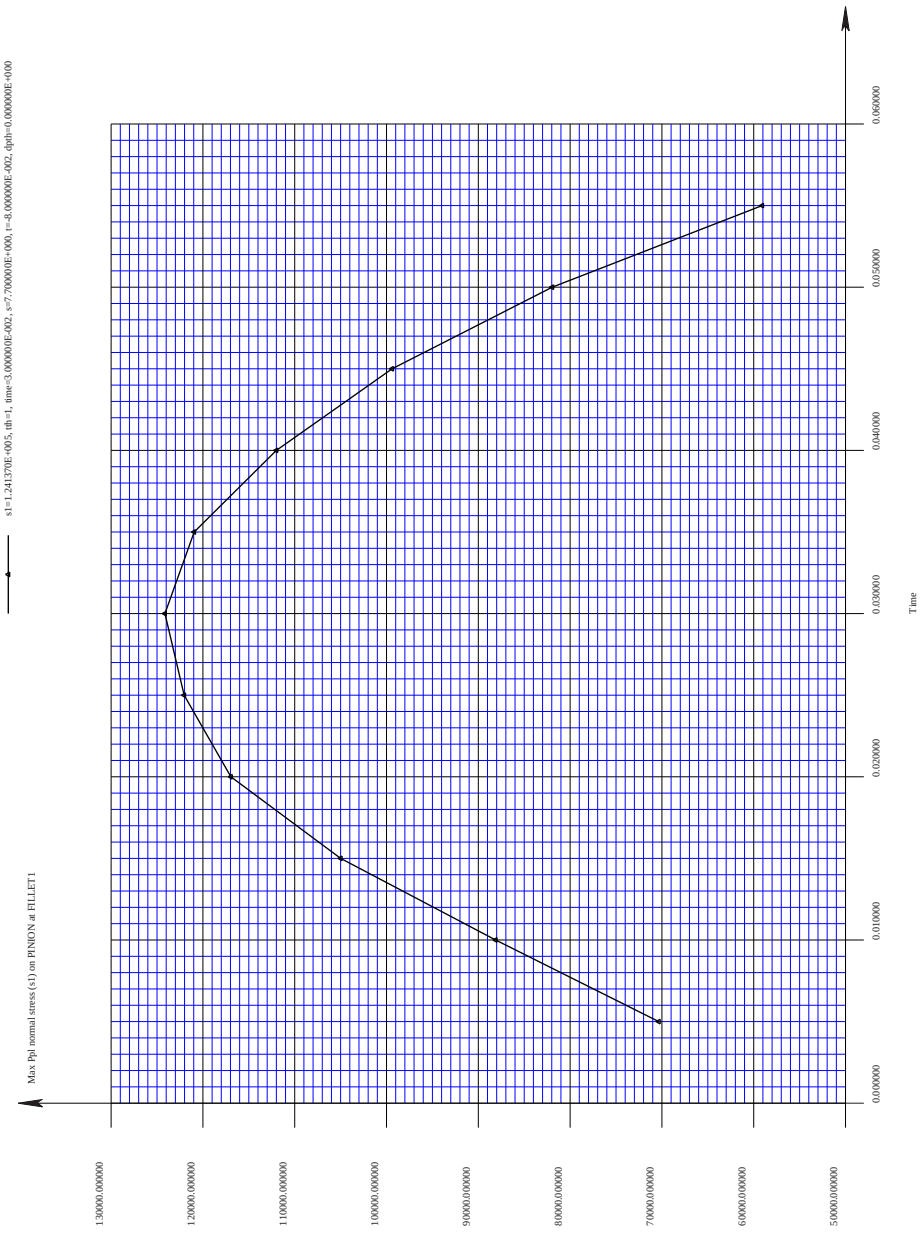

Figure 3.17: Plot of maximum principal normal stress against time for pinion tooth no.1 using the SEARCHSTRESS menu

Table 3.3: Searchstress data

Item	Description
COMPONENT	MAXPPLSTRESS
XAXIS	TIME
BEGINSTEP	1
ENDSTEP	11
BODY	PINION
SURFACE	FILLET1
TOOTHBEGIN	1
TOOTHEND	1
SEPTEETH	TRUE
SPROFBEGIN	6.00
SPROFEND	12.00
NUMSPROF	51
TFACEBEGIN	-0.5
TFACEEND	0.5
NUMTFACE	51
DEPTHBEGIN	0.00
DEPTHEND	0.00
NUMDEPTH	1
DISTMIN	0.05
OUTPUTTOFILE	TRUE
FILENAME	out.txt
APPEND	TRUE

Table 3.4: FE probe data

Item	Description
NPROBES	40
PROBE	1
BODY	PINION
MESH	TOOTH
ELEM	40
XI	0.433
ETA	1.00
ZETA	0.68
COMPONENT	MAXPPLNORMAL
FILENAME	PROBES.DAT

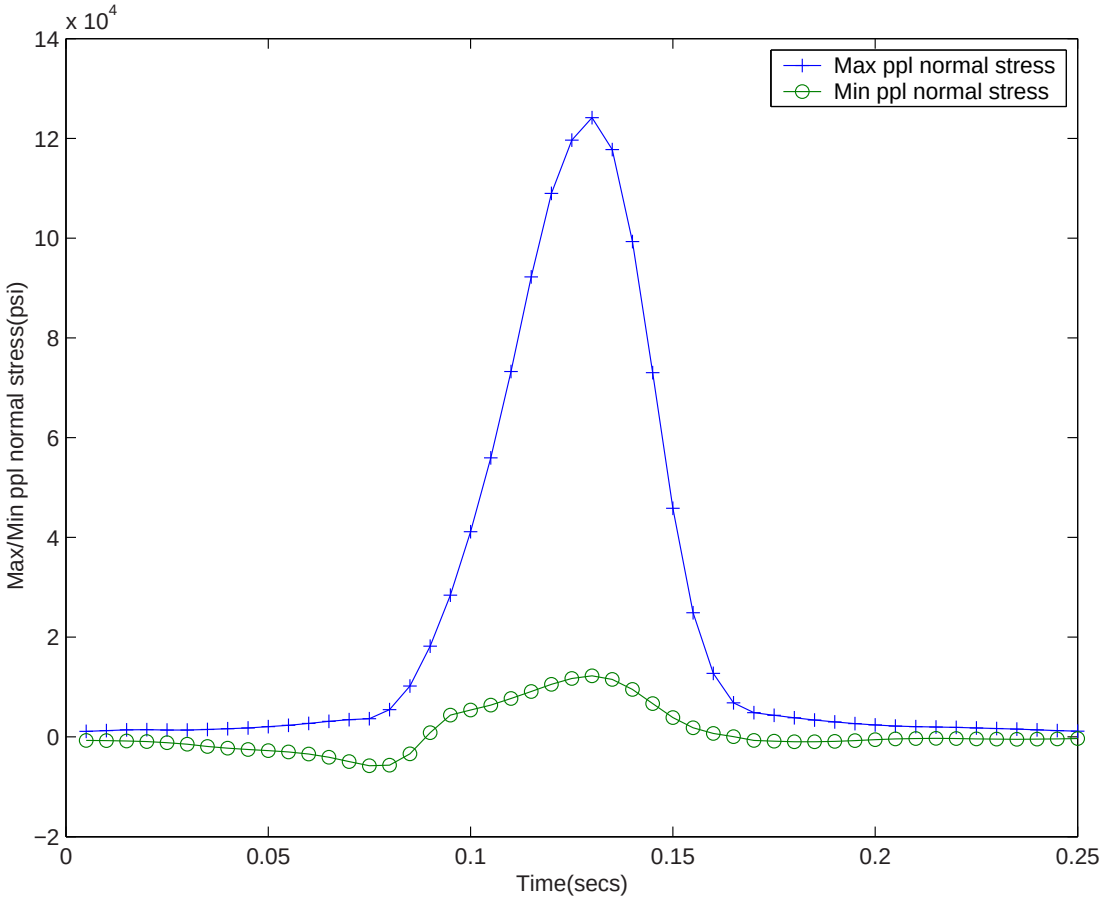

Figure 3.18: Plot of maximum and minimum principal stresses against time for pinion tooth for the case with rigid pinion inner diameter

3.9.2 Results

The maximum principal and the minimum principal normal stress plot obtained from the FE probe data is shown in Figure 3.18. The maximum principal normal stress $(\sigma_{\max}) = 1.24137 \times 10^5 psi$ and the minimum principal normal stress $(\sigma_{\min}) = -5.7812 \times 10^3 psi$. Hence, Alternating stress, $\sigma_{\mathrm{a}} = 6.4959 \times 10^4 psi$ and the Mean stress, $\sigma_{\mathrm{m}} = 5.9177 \times 10^4 psi$.

According to the Goodman's linear relationship, for a steel with tensile strength $180 kpsi$, the fatigue stress using above data is $96.774 kpsi$. Using an S-N plot for steel shown in Figure 3.16, the corresponding fatigue life is $4.75 \times 10^5 cycles$. Note that the S-N plot used in the figure is not a standard curve for gear materials. It is used to demonstrate the ability of the hypoid facemilled program in calculating the fatigue life.

3.10 Fatigue life for a thin flexible rim model

Load the file `fatiguethinrim.ses` located in the `FATIGUE` directory. The ISRACERIGID item is turned off for this example. The axial order and the circorder items are 2 and 4 respectively. In order to model the thin rim the BASESURFACETYPE is CONE with BASECONEANGLE(deg) as 13.00.

3.10.1 Locating the point of maximum stress

A plot of maximum principal stress against time for Pinion tooth no.1 is shown in Figure 3.19. Table 3.5 shows the searchstress menu to obtain this plot. Analysing the FE probe data the co-ordinates of the maximum stress point is found to be $(\xi, \eta, \zeta) = (0.386, 1.00, 0.70)$ on element no.40. For this point the plot of maximum and minimum principal normal stress against time is shown in Figure 3.20. An example of a FEPROBE menu is shown in Table 3.6.

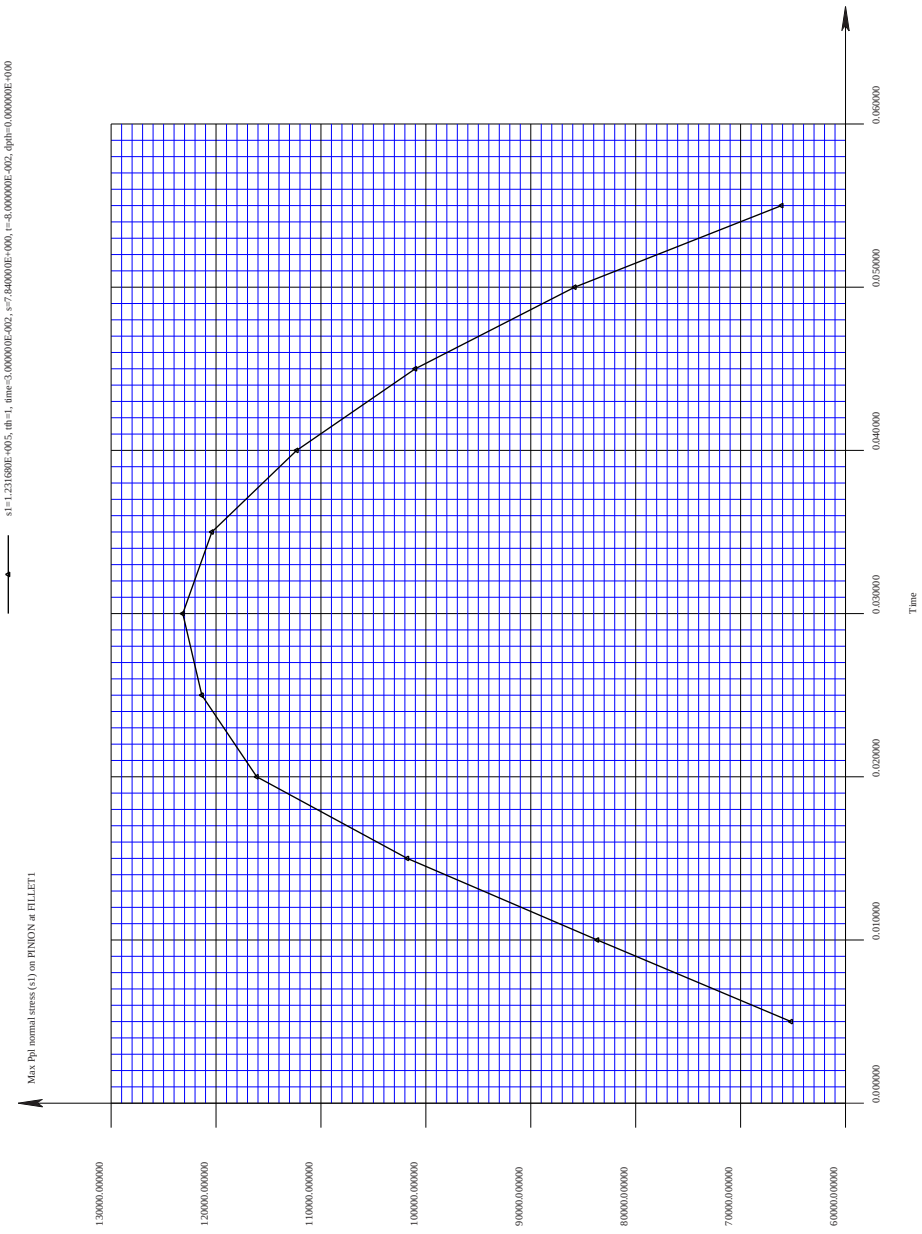

Figure 3.19: Plot of maximum principal normal stress against time for pinion tooth no.1 using the SEARCHSTRESS menu

Table 3.5: Searchstress data

Item	Description
COMPONENT	MAXPPLSTRESS
XAXIS	TIME
BEGINSTEP	1
ENDSTEP	11
BODY	PINION
SURFACE	FILLET1
TOOTHBEGIN	1
TOOTHEND	1
SEPTEETH	TRUE
SPROFBEGIN	6.00
SPROFEND	12.00
NUMSPROF	51
TFACEBEGIN	-0.5
TFACEEND	0.5
NUMTFACE	51
DEPTHBEGIN	0.00
DEPTHEND	0.00
NUMDEPTH	1
DISTMIN	0.05
OUTPUTTOFILE	TRUE
FILENAME	out.txt
APPEND	TRUE

Table 3.6: FE probe data

Item	Description
NPROBES	40
PROBE	1
BODY	PINION
MESH	TOOTH
ELEM	40
XI	0.386
ETA	1.00
ZETA	0.70
COMPONENT	MAXPPLNORMAL
FILENAME	PROBES.DAT

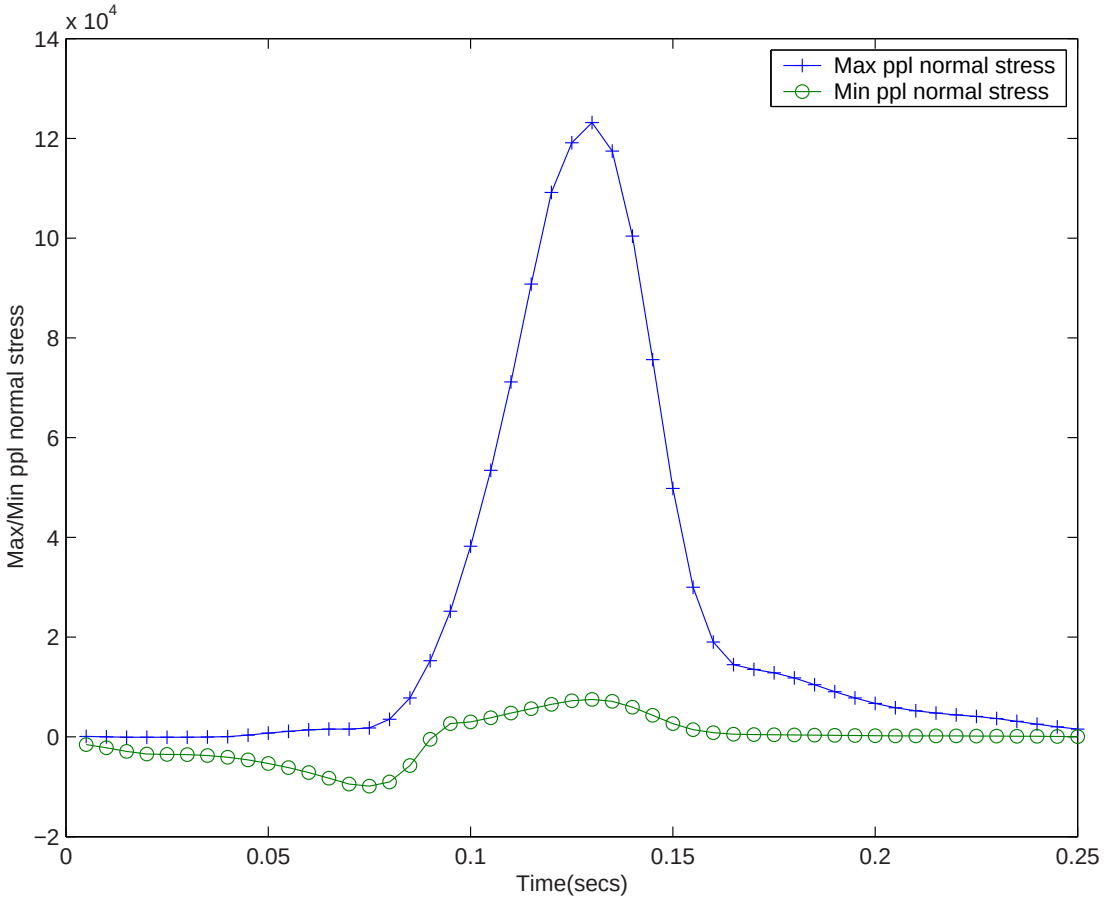

Figure 3.20: Plot of maximum and minimum principal stresses against time for pinion tooth for the case with thin flexible pinion inner diameter

3.10.2 Results

The maximum principal and the minimum principal normal stress plot obtained from the FE probe data is shown in Figure 3.20. The maximum principal normal stress ($\sigma_{\max}$) = $1.23168 \times 10^5 psi$ and the minimum principal normal stress ($\sigma_{\min}$) = $-9.869 \times 10^3 psi$. Hence, Alternating stress, $\sigma_{\mathrm{a}} = 6.6518 \times 10^4 psi$ and the Mean stress, $\sigma_{\mathrm{m}} = 5.6649 \times 10^4 psi$.

According to the Goodman's linear relationship, for a steel with tensile strength $180 kpsi$, the fatigue stress using above data is $97.066 kpsi$. The fatigue life for this stress is $4.6 \times 10^5 cycles$.

3.11 Cumulative damage

The S-N curves discussed in previous section are developed for constant stress amplitude operation. But, in virtually every engineering application where fatigue is an important failure mode, the alternating stress amplitude may be expected to vary or change in some way during the service life. Hence the usage of S-N curves in such cases is inapplicable. Therefore theories based on cumulative damage are used while predicting fatigue failure.

The fatigue damage produced at any given cyclic stress amplitude will be related to the total number of cycles of operation at that stress amplitude and also related to the total number of cycles that would be required to produce failure of an undamaged specimen at that stress amplitude. It is further postulated that the damage incurred is permanent and operation at several different stress amplitudes in sequence will result in an accumulation of total damage equal to the sum of the damage increments accrued at each individual stress level. When the total accumulated damage reaches a critical value, fatigue failure occurs. Many different theories based on this concept of cumulative damage have been proposed. We discuss here two theories very commonly used for the purposes of assessing fatigue damage.

3.11.1 Linear damage theory

The linear damage theory is also referred as the Plamgren-Miner hypothesis or the linear damge rule. As discussed earlier the S-N curve(Figure 3.21) at a constant stress amplitude S_1 will produce complete damage, or failure, in N_1 cycles. Operation at stress amplitude S_1 for a number of cycles n_1 smaller than N_1 will produce a smaller fraction of damage, D_1. D_1 is usually termed as the damage fraction. Operation over a spectrum of different stress levels results in a damage fraction $\mathrm{D_i}$ for each of the different stress levels $\mathrm{S_i}$ in the spectrum. When this damage fractions sum to unity, failure is predicted, that is,

Failure is predicted to occur if:

$$D_1 + D_2 + ... + D_{i-1} + D_i \geq 1 \tag{3.14}$$

The Palmgren-Miner hypothesis asserts that the damage fraction at any stress level $\mathrm{S_i}$ is linearly proportional to the ratio of number of cycles of operation to the total number of cycles that would produce failure at that stress level, that is

$$D_i = \frac{n_i}{N_i} \tag{3.15}$$

Thus we can also say that failure is predicted to occur if:

$$\frac{n_1}{N_1} + \frac{n_2}{N_2} + ... + \frac{n_{i-1}}{N_{i-1}} + \frac{n_i}{N_i} \geq 1 \tag{3.16}$$

or failure is predicted to occur if:

$$\sum_{j=1}^{i} \frac{n_j}{N_j} \geq 1 \tag{3.17}$$

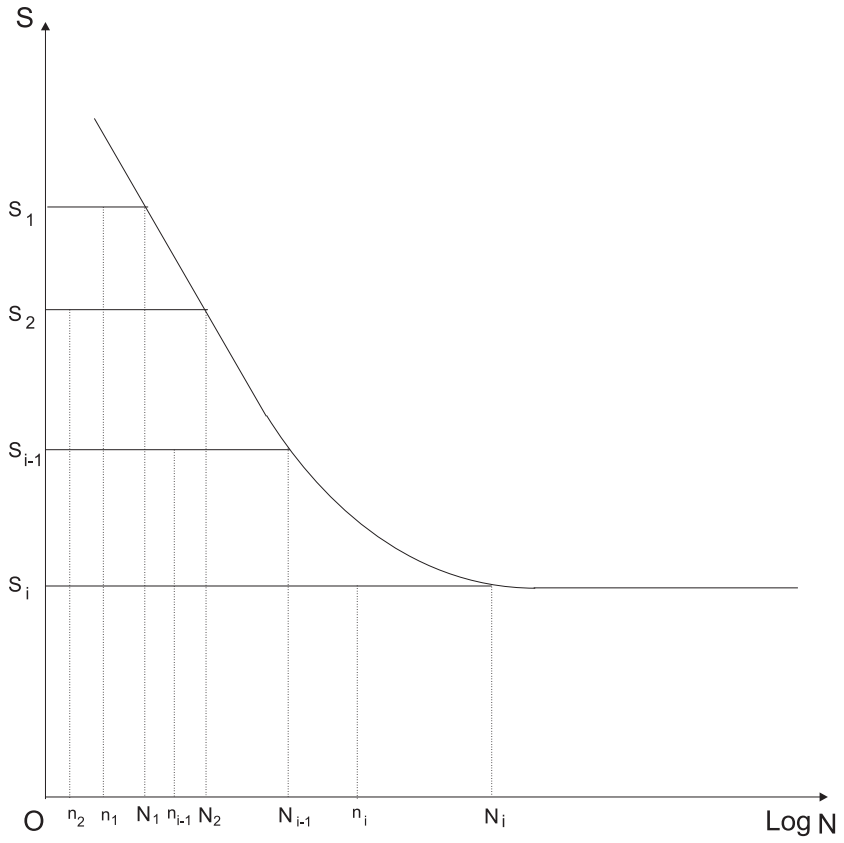

Figure 3.21: S-N plot illustrating the linear damage theory

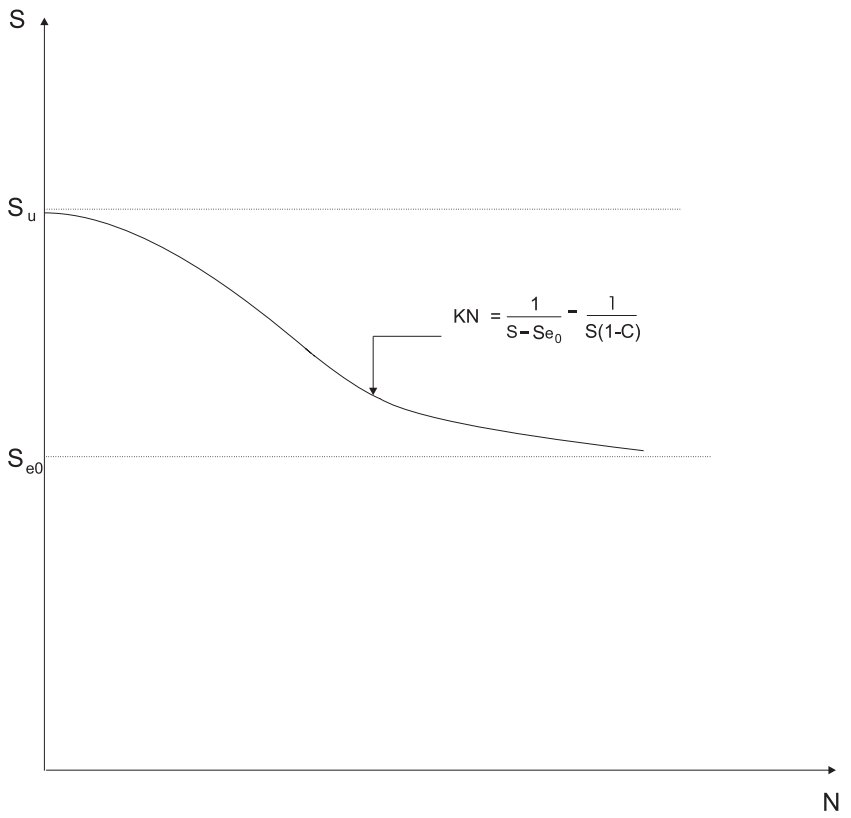

Figure 3.22: S-N curve approximation proposed by Gatt

The Palmgren-Miner hypothesis is widely used because of its simplicity and the experimental fact that the other much more complex cumulative damage theories do not always yield a significant improvement in failure prediction reliability. The most significant drawback of the theory though is that no influence of the order of application of various stress levels is recognized, and damage is assumed to accumulate at the same rate at a given stress level without regard to past history. Experimental data suggest that the order in which various stress levels are applied does have a significant influence and also that the damage rate at a given stress level is a function of the prior cyclic stress history.

3.11.2 Gatts Cumulative damage theory

Gatts postulated that the fatigue strength and the the fatigue limit change continuously with the application of stress cycles, and that the change is proportional to a function of the stress amplitude.

The S-N curve[3] according to the Gatt's theory is given as:

$$kN = \frac{1}{S - S_{e_0}} - \frac{1}{S(1 - C)} \tag{3.18}$$

where,

[3]See Failure of materials in mechanical design by J.A. Collins.

C, k = Material constant and proportionality constant
S_{e_0} = fatigue limit when N = 0
S_q = Instantaneous value of strength
S_e = Fatigue limit, a function of cyclic stress history, not a constant
= CS_q
N = Number of cycles of stress applied
S = Amplitude of applied cyclic stress

Figure 3.22 shows the S-N curve based on the Gatt's cumulative damage theory.

Knowing the material properties and calculating the stress amplitude from the FE probe data it is possible to calculate the fatigue life for a hypoid gear pair based on the Gatts cumulative damage theory.

3.12 Fatigue life based on duty cycle for a gear set

We assume the gear set shown in example file `fatigue.ses` to be running at 90% of the total torque.

Load the file `fatigueload1.ses` located in the `FATIGUE` directory. We now run the gear set at about 110% of the total load($Torque = 3194.07 lbf.in$). For this load the maximum sress plot from the search stress menu is shown in Figure 3.23. The maximum stress point using the FE probe data is found to be (0.50,1.00,0.62). For this point the maximum and minimum principal normal stress plot is shown in Figure 3.24. The corresponding fatigue life hence obtained is $6.0 \times 10^4 cycles$.

Load the file `fatigueload2.ses` located in the `FATIGUE` directory. We now run the gear set at 100% load($Torque = 2903.7 lbf.in$). For the point (0.50,1.00,0.62) on element no.40 the maximum and minimum principal normal stress plot is shown in Figure 3.25. The corresponding fatigue life hence obtained is $1.9 \times 10^5 cycles$.

Load the file `fatigueload3.ses` located in the `FATIGUE` directory. We now run the gear set at $Torque = 1500 lbf.in$. For the point (0.50,1.00,0.62) on element no.40 the maximum and minimum principal normal stress plot is shown in Figure 3.26. The corresponding fatigue life hence obtained is infinite.

Load the file `fatigueload4.ses` located in the `FATIGUE` directory. We now run the gear set at $Torque = 2613.33 lbf.in$. For the point (0.50,1.00,0.62) on element no.40 the maximum and minimum principal normal stress plot is shown in Figure 3.27. The corresponding fatigue life hence obtained is $4.5 \times 10^5 cycles$.

The load and the corresponding fatigue life is summarised in Table 3.7.

Table 3.7: Fatigue life for a duty cycle

Torque(lbf-in)	Fatigue life(cycles)	Number of cycles (%)
1500	∞	70%
2613.33	4.5e5	20%
2903.7	1.9e5	9%
3194.07	6.0e4	1%

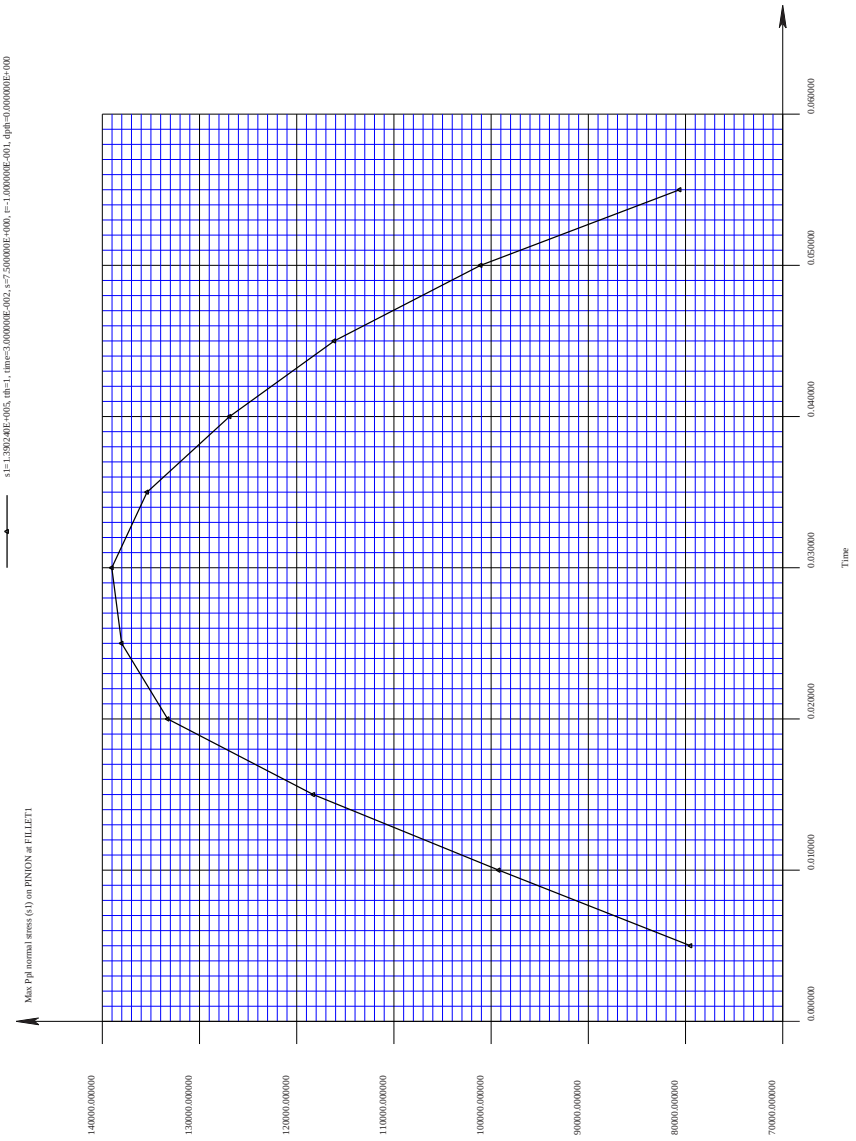

Figure 3.23: Maximum principal normal stress plot against time for pinion tooth no.1 for a output torque of 3194.07 lbf.in

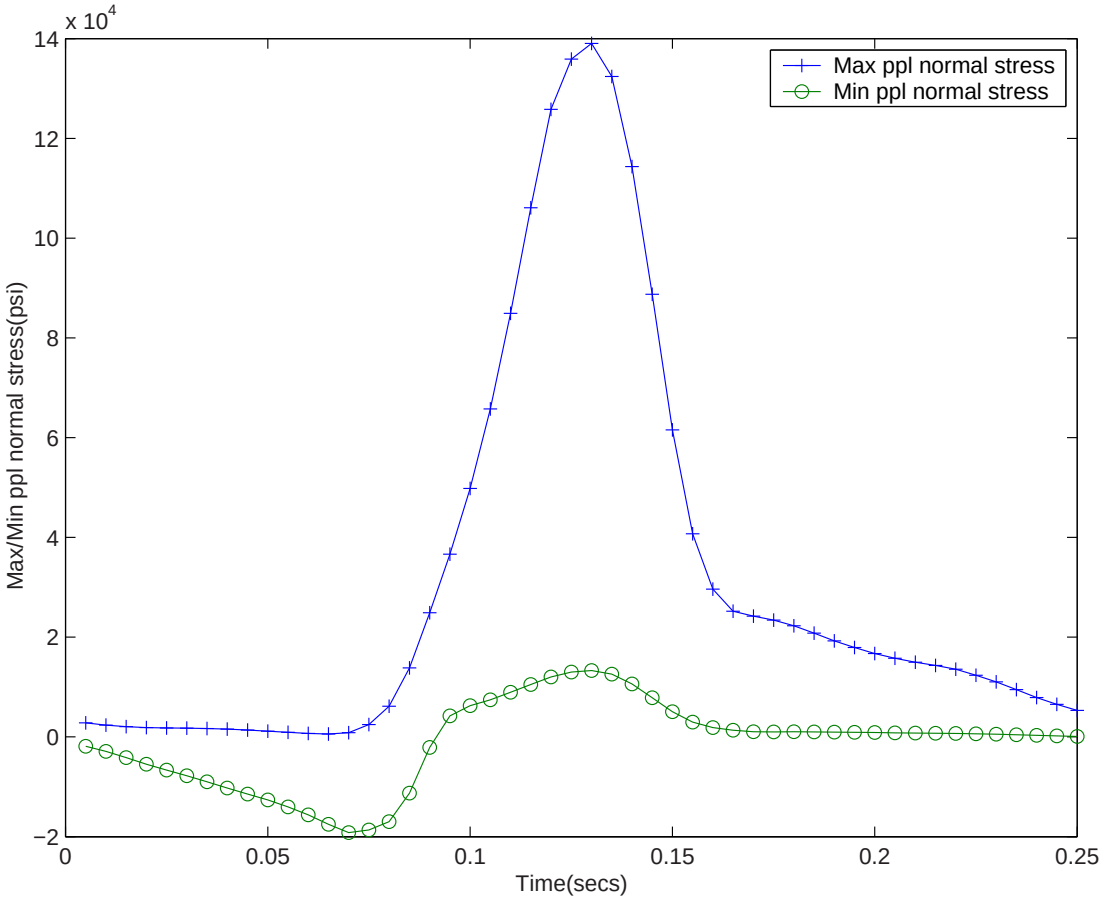

Figure 3.24: Maximum and minimum principal normal stress plot against time for pinion tooth for output torque of 3194.07 lbf.in

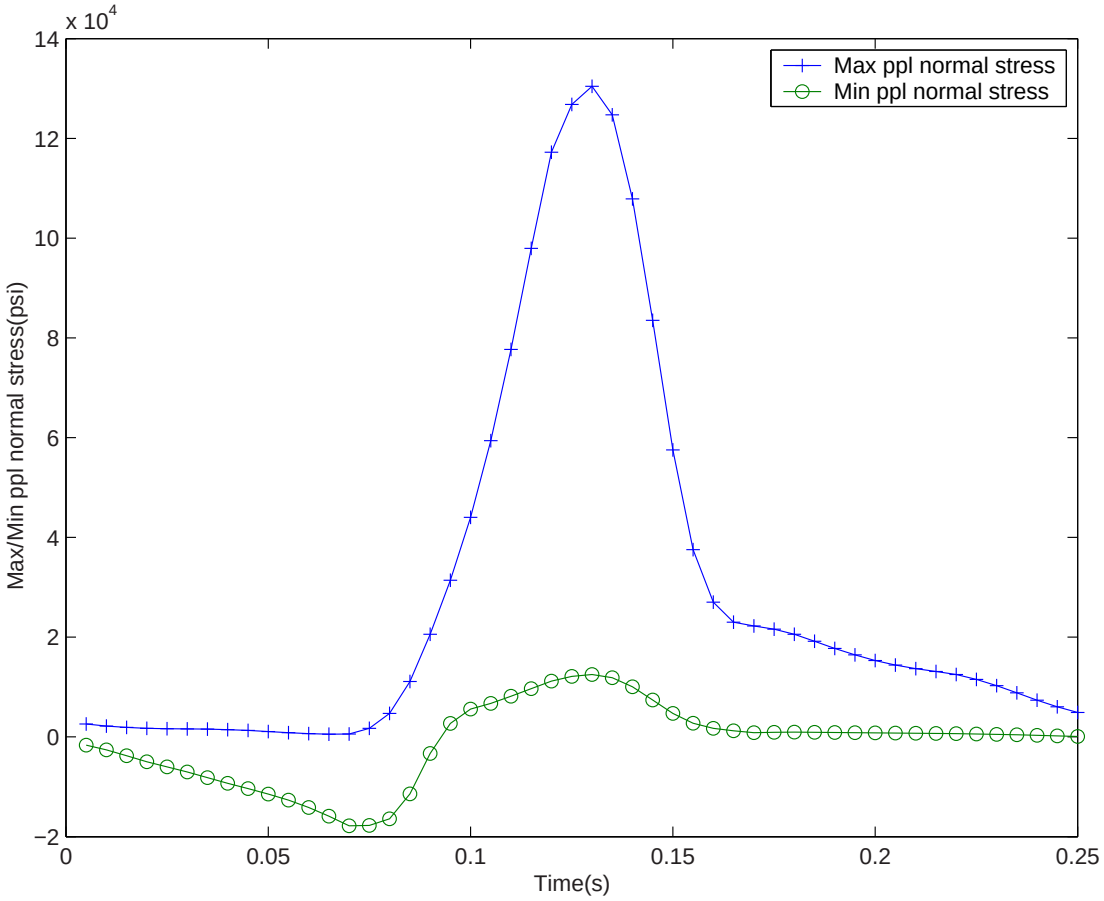

Figure 3.25: Maximum and minimum principal normal stress plot against time for pinion tooth for output torque of 2903.7 lbf.in

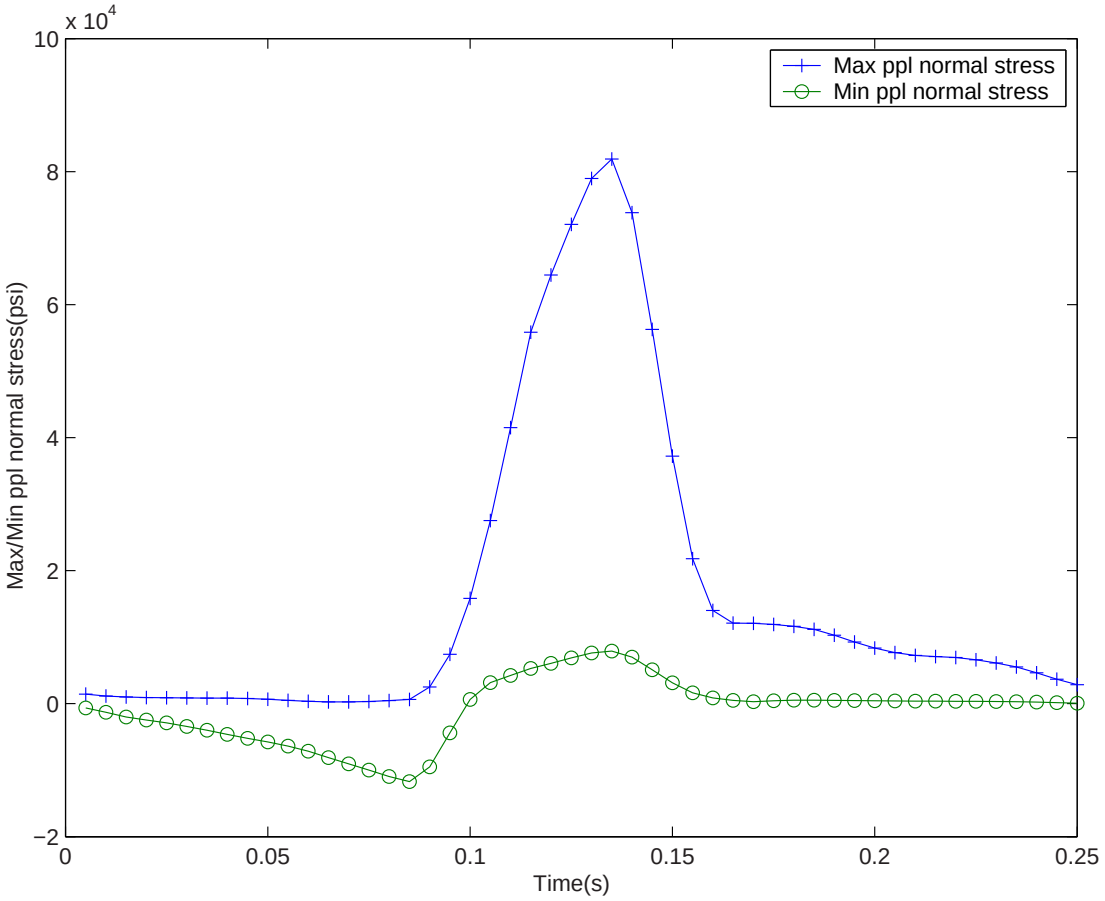

Figure 3.26: Maximum and minimum principal normal stress plot against time for pinion tooth for output torque of 1500 lbf.in

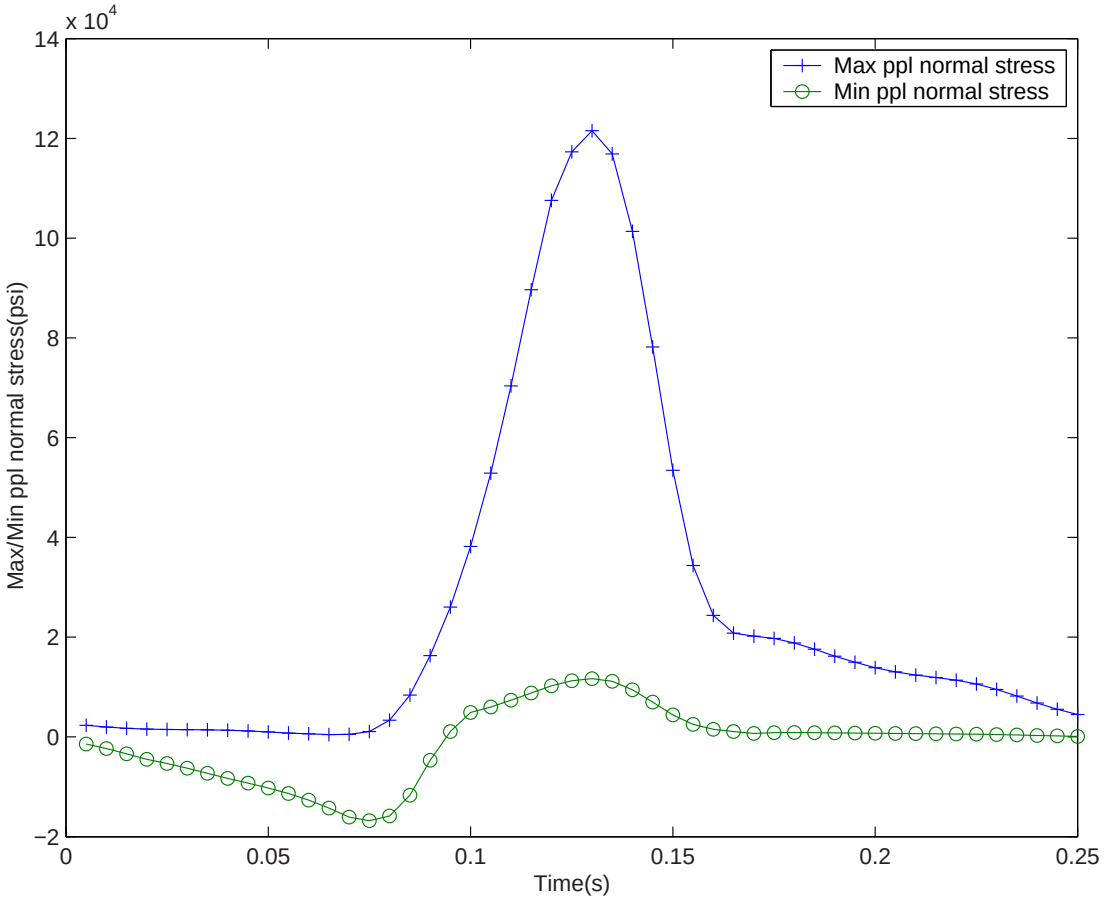

Figure 3.27: Maximum and minimum principal normal stress plot against time for pinion tooth for output torque of 2613.33 lbf.in

3.13 Calculating life based on cumulative damage theory

From the Linear damage theory failure occurs when:

$$\frac{n_1}{N_1} + \frac{n_2}{N_2} + ... + \frac{n_{i-1}}{N_{i-1}} + \frac{n_i}{N_i} = 1 \tag{3.19}$$

Substituting the values from Table 3.7 in the above we get:

$$\frac{0.7n}{\infty} + \frac{0.2n}{4.5 \times 10^5} + \frac{0.09n}{1.9 \times 10^5} + \frac{0.01n}{6.0 \times 10^4} = 1 \tag{3.20}$$

Thus, the life cycle for the gear set is $9.21832 \times 10^5 cycles$.

3.14 Summary

We have shown how the *Hypoid facemilled* program can be employed to calculate the fatigue life for gear bodies. As can be seen from the Table 3.7 as the load increases the fatigue life is found to decrease as expected.

Bibliography

[1] *Planetary Gear Train Ring Gear and Support Structure Investigation*, Mark Valco, Ph.D. Dissertation, Cleveland State University, 1992.

[2] *Gear Tooth Stress Measurements of Two Helicopter Planetary Stages*, Krantz, T. L., NASA Technical Memorandum 105651, AVSCOM Technical Report 91-C-038, 1992.

[3] A combined surface integral and finite element solution for a three-dimensional contact problem, S. Vijayakar, *International Journal for Numerical Methods in Engineering*, vol.31, pp. 525-545, 1991.

[4] *Nonlinear and dynamic programming*, G. Hadley, Addison Wesley Publishing company, 1964.

[5] *Linear programming*, George Hadley, Addison Wesley, 1962.

[6] *Linear and Combinatorial Programming*, Katta G. Murty, John Wiley, 1976 ISBN: 0-471-57370-1.

[7] Linearization of multibody frictional contact problems, S. Vijayakar, H. Busby and D. Houser, *Computers and Structures*, vol. 29, no. 4, pp. 569-576, 1987.

[8] *Natural Frequency Spectra and Vibration Modes of Planetary Gears*, Jian Lin and Robert Parker, 1998 ASME Design Engineering Technical Conference, September 1998, Atlanta Georgia.

[9] *Gear Dynamics Experiments, Part I: Characterization of Forced Response*, Blankenship and Kahraman, ASME 7^{th} International Power Transmissions and Gearing Conference, San Diego, October 1996.

[10] *Gear Dynamics Experiments, Part II: Effect of Involute Contact Ratio*, Blankenship and Kahraman, ASME 7^{th} International Power Transmissions and Gearing Conference, San Diego, October 1996.

[11] *Gear Dynamics Experiments, Part III: Effect of Involute Tip Relief*, Blankenship and Kahraman, ASME 7^{th} International Power Transmissions and Gearing Conference, San Diego, October 1996.

[12] The use of boundary elements for the determination of the geometry factor, Vijayakar and Houser, 1986 *AGMA Fall Technical Meeting*, Paper no. 86-FTM-10.

[13] Finite element analysis of quasi-prismatic structures, S. Vijayakar, H. Busby and D. Houser, *International Journal for Numerical Methods in Engineering*, vol. 24, pp. 1461-1477, 1987.

[14] Edge effects in gear tooth contact, S. Vijayakar, *ASME 7^{th} International Power Transmissions and Gearing Conference*, San Diego, October 1996.

[15] Vibration Measurements on Planetary Gears of Aircraft Turbine Engines, M. Botman, *AIAA Journal*, vol. 17, no. 5, 1980.

[16] Dynamic Tooth Loads in Epicyclic Gears, F. Cunliffe, J. D. Smith, and D.B. Welbourn, *J. Eng. Ind. Trans. ASME*, May 1974.

[17] Effect of Internal Gear Flexibility on the Quassi-Static Behavior of a Planetary Gear Set, A. Kahraman, S. Vijayakar, *Transactions of the ASME*, September 2001.

[18] Bending strength estimation of thin-rimmed spur gears, Oda, Miyachika, *Transactions of the ASME*, October 1996.